Department Radiation Science & Technology
Section Nuclear Energy and Radiation Applications
Faculty of Applied Sciences
Delft University of Technology
Mekelweg 15, 2629 JB Delft
The Netherlands

Modeling and analysis of a depressurized loss of forced cooling event in a thorium fueled high temperature reactor

Bachelor thesis

Chris Graafland

18 March 2014

Supervisors:
Dr. ir. J.L. Kloosterman

Ir. F.J. Wols

List of Symbols

β^-	Beta decay [-]
ε	Emissivity coefficient [-]
η	Decay heat fraction [-]
λ	Heat conductivity coefficient [$Wm^{-1}K^{-1}$]
ρ	Density [kgm^{-3}]
σ	Stefan-Boltzmann constant [$Wm^{-2}K^{-4}$]
ϕ_q	Heat flow [W]
$\phi_q^{'}$	Heat flow per unit height [Wm^{-1}]
$\phi_q^{''}$	Heat flux [Wm^{-2}]
A	Area [m^2]
c_p	Specific heat capacity [$Jkg^{-1}K^{-1}$]
f	Weighting factor in time discretization [-]
H	Height reactor core [m]
P	Power [W]
q	Heat production [W]
S	Source term [W]
t	Time [s]
T	Temperature [K]
V	Volume [m^3]

Abstract

The pebble-bed reactor is a promising next generation nuclear reactor design. Generation IV reactor designs are designed to be inherently safe, so in all scenarios the reactor should be able to remove the decay heat by passive means only. The pebble-bed consists of 420,000 pebbles, where in each pebble fuel kernels are contained in so called TRISO particles. The nuclear fuel, the fission products and actinides, can effectively be retained inside the TRISO particles for temperatures up to 1600 ^{o}C. In this thesis the thorium breeder pebble-bed reactor is considered. Thorium is used as a fertile material to breed U-233. Thorium is three times more abundant on earth than uranium, but it is not fissile itself. This thesis analyzes a depressurized loss of forced cooling event in a uranium fueled HTR-PM and in a thorium breeder pebble-bed reactor.

For this purpose, two one-dimensional heat transfer models are developed in MATLAB. A steady state heat flux model, which gives a first insight in the radial temperature profile, and a time-dependent finite volume model, which solves the time-dependent heat equation. The heat flux model serves to validate the spatial discretization of the finite volume model. The finite volume model is used for the loss of forced cooling calculations, where instant depressurization to 1 bar and instant control rod insertion are assumed.

In the finite volume MATLAB model, the radial temperature profile of the uranium fueled HTR-PM and the thorium breeder PBR are compared. In the thorium PBR higher maximum fuel element temperatures and larger temperature differences across the core are reached for similar fuel irradiation times. Results of the finite volume MATLAB model are compared to THERMIX models by Zheng and Wols, for respectively the uranium fueled HTR-PM and the thorium breeder PBR. Similarities and differences are observed. The temperature profiles in the results look very similar. However, in the THERMIX models a higher maximum fuel element temperature is observed and a larger temperature difference across the core is observed. A reason for these differences might be a different implementation of the parameters within the THERMIX and the MATLAB models. To see how the design parameters influence the maximum temperature, a parameter sensitivity analysis is performed.

Contents

Chapter 1 Introduction

1.1. World energy demand

The world energy demand is expected to keep rising in the following decades. In 2035 the world energy demand will have increased by one-third according to the International Energy Agency. Approximately 90% of this increase will be due to emerging economies in South-East Asia and India. Fossil fuels, the main source of energy, currently account for 82% in the world's energy mix. [1] At present time, fossil fuels are abundantly mined and it is easier to use these fuels than any other energy source. This makes fossil fuels popular, especially in the fast growing economies. However, fossil fuels are running out and are therefore not a sustainable energy source. Furthermore, when fossil fuels are burnt pollutants are released. These pollutants include greenhouse and toxic gases, such as: carbon dioxide, nitrogen oxides, sulphur oxides and ash. For these reasons, alternative sustainable energy sources capable to meet the world energy demand are required.

Nuclear fission can be one of these alternative energy sources. In a nuclear fission reaction, after absorbing a neutron, a nucleus of a heavy element splits into smaller nuclei, releasing energy. When the heavy particle splits several neutrons are released. In a nuclear chain reaction these free neutrons can be absorbed in other nuclei and cause fission. Figure 1.1 represents a schematic overview of a nuclear chain reaction for U-235. In a nuclear power plant under normal operation the chain reaction happens in a controlled manner. The smaller nuclei are called the fission fragments. The fission fragments have high kinetic energies. Inside the fuel elements these high energy fission fragments bump into each other generating heat. In a nuclear reactor this heat is transferred to a liquid or a gas that flows around the fuel elements, called the coolant. The coolant drives turbines and electricity is generated. Very common uranium and plutonium are used as nuclear fuels.

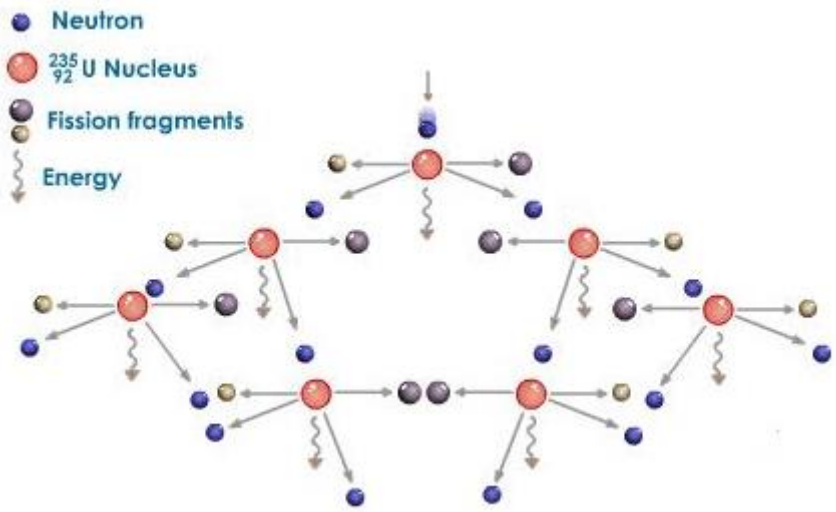

Figure 1 Schematic overview of the nuclear chain reaction with U-235.

Currently there are 436 nuclear reactors in operation and there are 72 nuclear reactors under construction [2]. In 2011 the world's nuclear reactors supplied 13% of the global electricity consumption [3]. The main advantages of nuclear energy is that less atmospheric pollutants and greenhouse gases are emitted in comparison with fossil fuels and that nuclear fuels are much more abundant on earth. Still, the public and political opposition is too strong to call nuclear energy the favorable sustainable energy source at present. Accidents in the past and the storage issue of nuclear waste make the general population think that nuclear energy is a dangerous energy source.

1.2. Concerns about nuclear safety

The great risk in a nuclear power plant is that large amounts of heat can be produced in a small volume in a very short time. Even when the nuclear chain reaction is stopped decay heat from the fission fragments can cause a core meltdown. In an incident scenario the chain reaction has to be stopped and the decay heat has to be removed properly. In the past there have been three major reactor accidents. These are the accidents of Three Mile Island, Chernobyl and Fukushima. On Three Mile Island and in Fukushima a loss of coolant accident occurred and the decay heat was not removed properly causing a core meltdown. In Chernobyl the nuclear chain reaction got out of control. In the three accidents radioactive materials were released into the environment. The accidents contributed to a negative public opinion with regard to nuclear energy and a decline in newly built nuclear reactors.

Nuclear power plant technology is not failure proof. Unexpected behavior of a nuclear reactor can cause high power outputs. Unforeseen events can slow down or stop the heat removal systems, this for example happened in Fukushima where an earthquake was followed by a tsunami. Miscalculations by plant operators and errors in computer driven system can cause accident scenarios. All of these uncertainties contribute to public and political opposition to nuclear energy. Other contributors are terrorism and the storage of nuclear waste issue. People are afraid that nuclear power plants are easy targets for terrorist attacks and that nuclear materials get into the wrong hands. Nuclear waste can remain radioactive for thousands of years. This waste has to be handled with great care and it has to be disposed in special engineered facilities.

1.3. Generation IV reactors

One of the most crucial safety features for a nuclear power plant is the ability to remove the heat produced in the reactor core under all circumstances, also when the cooling systems fail. In the nuclear accidents on Three Mile Island and in Fukushima, the heat removal systems failed to remove the produced heat properly. Nowadays researchers focus on inherently safe nuclear reactors. These reactors are able to remove decay heat by passive means in an emergency scenario.

An international group called the Generation IV International Forum (GIF) carries out research and development on the next generation of nuclear reactors, the Generation IV reactors. The GIF selected six nuclear reactors for further development: the Gas-cooled fast reactor, the Very-high-temperature reactor, the Supercritical-water-cooled reactor, the Sodium-cooled fast reactor, the Lead-cooled fast reactor and the Molten salt reactor. In Figure 2, these reactors are schematically displayed. The main areas of improvement compared to Generation III reactors are on inherent safety, proliferation resistance, economically competitiveness and on minimizing nuclear waste [4].

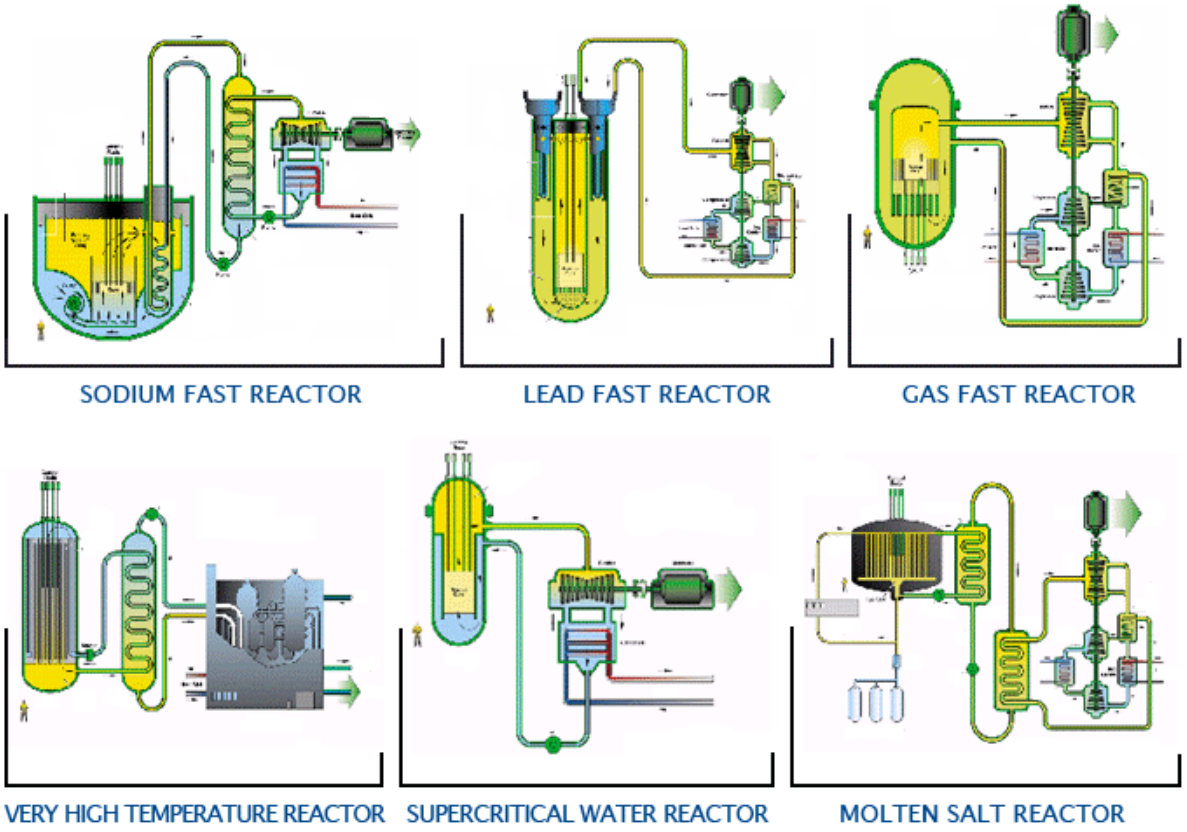

Figure 2 Overview of the Generation IV nuclear reactors proposed by the GIF. Source: http://www.euronuclear.org

1.4. The High Temperature Reactor Pebble-bed Module

One of the six nuclear reactor types proposed by the GIF is the very high temperature reactor (VHTR). This is an improved design of the high temperature gas cooled reactor (HTGR). In a HTGR the coolant outlet temperatures lie between 700 °C and 900 °C, while in a VHTR coolant outlet temperatures are even higher. Nuclear reactors with higher outlet temperature reach higher thermal efficiency and are attractive for hydrogen production [4]. The HTGR has been developed for nearly 60 years now [5]. The HTGR has two main types of core configurations: the pebble-bed and the prismatic block core configuration, in this thesis the main focus will be on the pebble-bed configuration. In this configuration the fuel particles are contained in small spheres, called pebbles. HTGR's offer several

advantages in comparison with the common Pressurized Water Reactors and the Boiling Water Reactors. HTGR's have a higher thermal efficiency. Also, the reactor design is inherently safe when the maximum fuel element temperature stays below 1600 °C. The reasons for this are that the design has negative temperature feedback coefficients and that the radioactive fission products are retained in the fuel particles for temperatures up to 1600 °C [7].

Three well-known pebble-bed reactors in history are the Arbeitsgemeinschaft Versuchsreaktor (AVR) in Germany, the thorium high temperature reactor of 300 MW electrical power (THTR-300) in Germany and the HTR-10 in China. These reactors were mainly demonstration plants and they were not commercial viable. On the other hand the safety experiences with these reactors were positive [9].

More than 30 years ago the concept of a modular high temperature gas-cooled reactor (MHTGR) was proposed. The concept of the MHTGR is to combine standardized HTGR reactor units with thermal power ratings of 200 MW, called modules, to form nuclear reactors of any desired power output [10]. The MHTGR is attractive because of its inherent safety features. Due to the geometry of the modules, that is a small radius compared to the height, decay heat can easily escape in comparison with larger reactor cores. Furthermore, the modular design offers market flexibility. Modular reactor systems are expected to cost less than reactors of comparable power ratings [11]. South Africa, the USA, Russia, Japan, France and especially China are currently constructing or planning projects for this type of modular reactor [5].

In China the economy grows rapidly and it seems inevitable to invest in nuclear energy. The first MHTGR demonstration plant, the high temperature reactor pebble-bed module (HTR-PM), was planned to be finished in 2012. Construction plans of the HTR-PM in Shidaowan were delayed due to the nuclear disaster in Fukushima [13]. Supported by the Chinese National High Technology Program, whose main tasks is to achieve breakthroughs in sustainable energy development, a 10 MW HTGR was constructed, the HTR-10 [12]. In January 2003 the HTR-10 operated at full power. A next step is to construct a commercial HTR-PM in Shidaowan [5]. Two 250MW_{th} reactors, based on the HTR-10 prototype, will be connected to the same steam turbine.

1.5. Thorium

An alternative to the common nuclear fuel uranium in the HTR-PM is the thorium isotope, Th-232. Thorium is approximately three times more abundant on earth than uranium. Another advantage is that in the thorium fuel cycle less long lived minor actinides are produced. Thorium however is not fissile itself. In a so called breeder reactor Th-232 is converted to U-233, after capturing a neutron followed by two beta decays. In a breeder reactor more U-233 is produced than consumed.

$$^{232}_{90}Th + n \longrightarrow {}^{233}_{90}Th \xrightarrow{\beta-} {}^{233}_{91}Pa \xrightarrow{\beta-} {}^{233}_{92}U \tag{1.1}$$

A thorium fueled HTR-PM design is proposed by Wols et al. [6], which will be elaborated on later in this thesis.

1.6. Outline

For a high temperature reactor a depressurized loss of forced cooling (DLOFC) event is a worst case design basis accident. It is crucial for the introduction of the HTR-PM worldwide that the reactor remains safe during such an event, that is the fuel temperature does not exceed 1600 ^{o}C. In a DLOFC event a rapid depressurization is assumed due to a rupture of a main coolant pipe. The dominant heat transfer mechanisms to remove the decay heat are conduction and radiation, since heat transfer by convection is negligible at a pressure of 1 bar.

A depressurized loss of forced cooling accident analysis is already done by Chinese researchers for a uranium fueled HTR-PM [7]. In this thesis a DLOFC event analysis for a thorium breeder pebble-bed reactor [14], based upon the HTR-PM, will be presented. The main question is whether the decay heat can be removed by passive means only in this reactor in case of a depressurized loss of forced cooling event.

First a steady state temperature profile is obtained using a heat flux model. This model is for a first insight in the temperature profile.

Secondly, a DLOFC transient in a uranium fueled HTR-PM will be simulated. In this model the finite volume method (FVM) is used to discretize the heat equation and the tridiagonal matrix algorithm (TDMA) is used to solve the algebraic linear equations [15,16]. The discretization will be validated using the steady state heat flux model from the previous paragraph. The DLOFC transient model will be compared with transient studies of the Chinese 200 MWe HTR-PM by Zheng et al. [7]. A sensitivity analysis will be done to see how the different parameters influence the maximum temperature.

Thirdly, a DLOFC transient in a thorium breeder pebble-bed reactor will be simulated using the FVM MATLAB model. These transient studies will be compared to the models of Wols [14] and to the transient in the uranium fueled HTR-PM. It will be verified whether the temperatures stay under the temperature limits of the main components in the reactor. Different decay heat models will be used to see how this affects the maximum temperature in the thorium PBR. Furthermore, a literature study is performed to look for decay heat models of U-233.

In Chapter 2 the technological aspects and the geometries of the HTR-PM are presented. Also, the physical aspects of the heat transfer models are introduced and the different decay heat models are presented in this chapter. The developed numerical models are presented in Chapter 3. In Chapter 4 the results are presented and in Chapter 5 conclusions are drawn.

Chapter 2 Theory

2.1. The thorium fueled high temperature reactor pebble-bed module

The high temperature reactor pebble-bed module (HTR-PM) consists of two modular gas-cooled high temperature reactors of 250 MW thermal power [7]. The modules have separate, but identical reactor buildings. Each reactor building contains three pressure vessels. The reactor pressure vessel (RPV) and the steam generator pressure vessel (SGPV) are connected by the hot gas duct pressure vessel (HDPV). The helium blower and the steam generator are located in the SGPV. Helium is used as coolant because, it is extremely inert from a chemical and neutron physical viewpoint [10]. Another advantage is that helium has a high heat capacity compared with other gases, which is good for heat transfer. In the primary loop cold helium flows from the helium blower, through the gas duct, to the RPV where the reactor core is located. The helium flows through the side reflector to the top of the core and flows down through the core taking up the fission heat. The heated helium flows back to the SGPV via the gas duct. After passing the steam generator the helium returns to the helium blower completing a cycle in the primary loop. Typical helium core inlet and outlet temperatures are 250 °C and 750 °C, respectively. [8] In Figure 3 the cross section of the HTR-PM is shown.

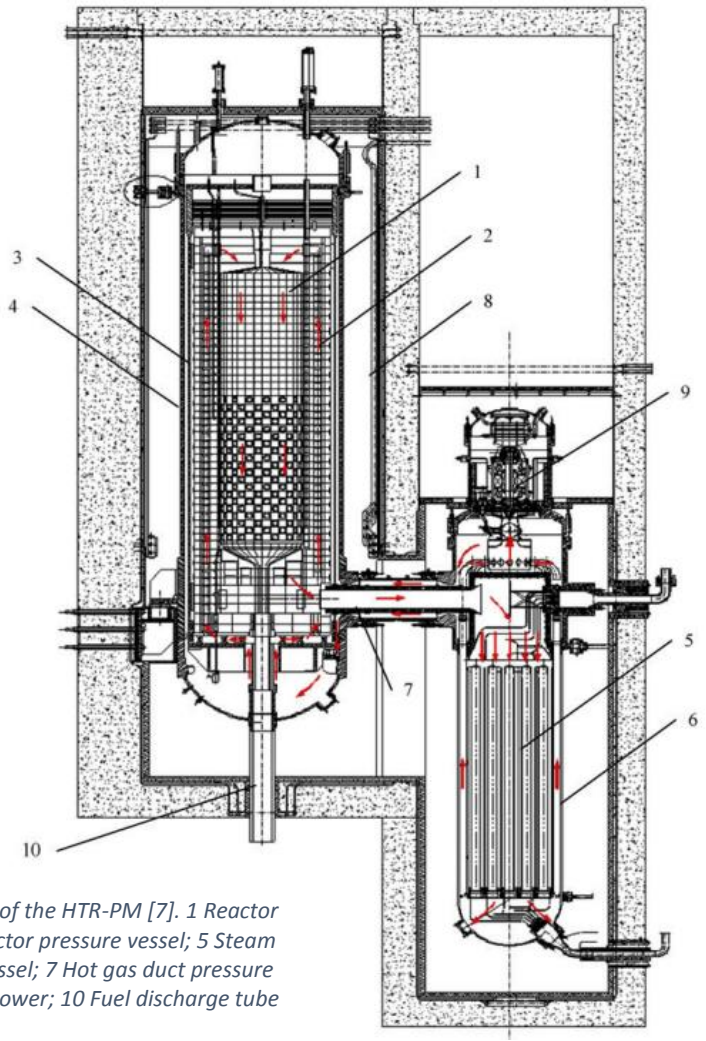

Figure 3 Cross section of the primary loop of the HTR-PM [7]. 1 Reactor core; 2 Side reflector; 3 Core barrel; 4 Reactor pressure vessel; 5 Steam generator; 6 Steam generator pressure vessel; 7 Hot gas duct pressure vessel; 8 Water-cooling panel; 9 Helium blower; 10 Fuel discharge tube

In the RPV the cylindrical pebble-bed core is located. The core is a randomly packed bed with approximately 420,000 pebbles. The pebbles are 6 cm in diameter. Inside each pebble there are 12,000 spherical TRISO coated particles, embedded in a graphite matrix. The graphite functions as moderator. The TRISO particles, 0.92 mm in diameter contain the nuclear fuel surrounded by several pyrolytic carbon and silicon carbide layers. A schematic overview of a pebble is given in Figure 4. These TRISO particles can effectively retain the fission products for temperatures up to 1600 °C. This greatly contributes to the inherent safety of the HTR-PM. Two other main contributors to the inherent safety are that pebble-bed reactors are designed with negative temperature coefficients, so the reactor itself reacts to certain malfunctions [12] and the geometry of the reactor. Due to the small radius compared to the height of the reactor core, decay heat is removed more easily than in larger reactors. [7]

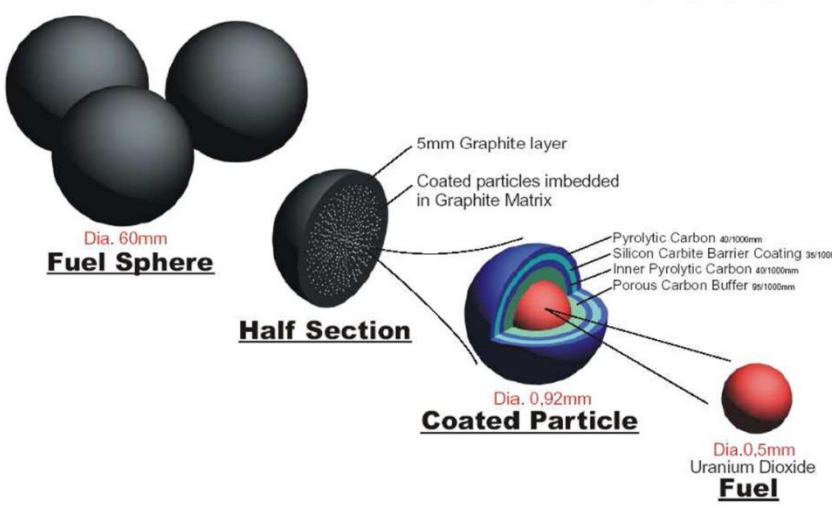

Figure 4 Schematic overview of the inside of a pebble in the HTR-PM. Source: www.nuclearstreet.com

A thorium fueled HTR-PM design is proposed by Wols et al. [6]. The proposed core model consists of a breeder zone and a central driver zone. Fuel pebbles inserted in the breeder zone contain Th-232 only. Here the thorium isotopes are partly converted into fissile U-233. The fuel pebbles in the driver zone contain 90% Th-232 and 10% U-233. In the driver zone the fissile U-233 is burnt to sustain the chain reaction and the excess fission neutrons convert thorium or cause fission.

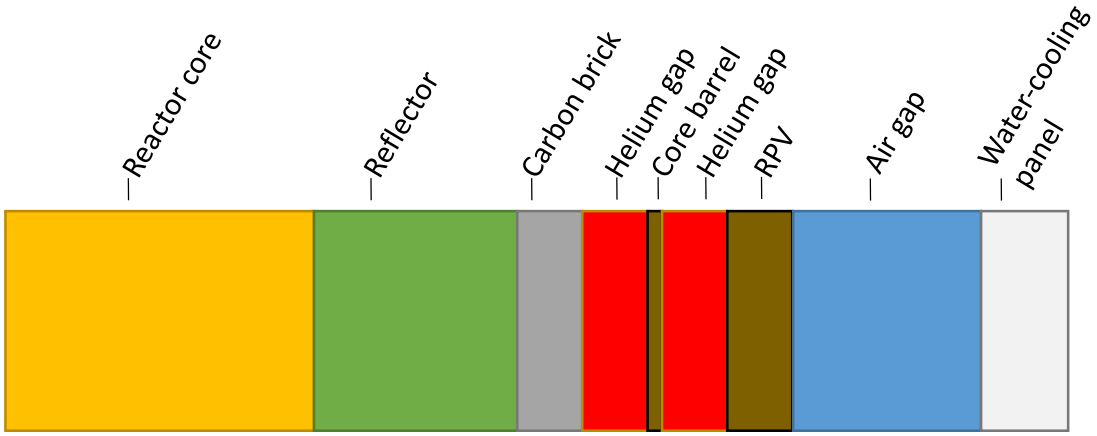

Figure 5 One-dimensional radial model of the pebble-bed reactor used to calculate the heat transfer from the core to the surroundings

In this thesis the heat transfer from the core to the surroundings is simulated one- dimensionally in the radial direction. The components above and under the reactor core are neglected in the heat transfer models, since in these components no maximum or critical temperatures are reached. In Figure 5 the reactor components in the radial direction are shown. In the thorium fueled HTR-PM the inner region of the reactor core is the driver zone and the outer region is the breeder zone. The reactor core is surrounded by a ceramic structure: the side reflector and the carbon brick. The reflector reflects neutrons into the core and reduces neutron leakage. The carbon brick has a supportive function and it protects the reactor components further away from the core against too high temperatures. The ceramic structure is surrounded by the metallic core barrel and the metallic RPV, these layers support the ceramic structure. The metallic layers are protected against heat from the core by several helium gaps and the carbon brick [8]. The RPV is surrounded by the air gap and the water-cooling panel. This water-cooling panel is kept at 70 ^{o}C, so the strength of the concrete surrounding the RPV is guaranteed. The water-cooling panel functions as residual heat removal system (RHRS). It transfers the heat to the air-water heat exchangers where the heat is finally transferred to the atmosphere. In Table 1 the temperature limits of the main components in the reactor are listed [7]. In Appendix A, the main design parameters and the reactor dimensions are summarized.

Table 1 Temperature limits of the main components in the HTR-PM

Component	Temperature during normal operation (^{o}C)	Temperature limits in accident (24 hours) (^{o}C)
TRISO particles	1100	1600
RPV	350	400
Core barrel	350	500
Reactor cavity concrete	70	100

2.2. Depressurized loss of forced cooling event

The worst case of a loss of forced cooling event is a depressurized loss of forced cooling (DLOFC) event. In a DLOFC event analysis it is assumed that the coolant stops flowing, because of a ruptured coolant pipe. When this happens the fission chain reaction will be shut down in a couple of seconds as the control rods are inserted. The model assumptions are that the depressurization and the control rod insertion take place at zero time. It is assumed that there is no air-ingress due to the ruptured coolant pipe. This is a core conduction heat up event. The helium pressure under normal operation conditions is 70 bar. In a DLOFC event the helium pressure drops to 1 bar. Therefore heat transfer by convection, the dominant transport mechanism under steady state conditions, is negligible. The dominant ways to remove the decay heat become heat transfer by conduction and radiation. These processes remove the heat slower than convection, therefore the temperatures of the reactor components, especially the fuel, will rise substantially [7].

2.3. Steady state heat flux model

In the ceramic and metallic layers of the HTR-PM model heat conduction is the dominant way of heat transfer. Heat conduction in a cylinder is described by Fourier's law [17] as shown in (2.1).

$$\phi''_{q,r} = -\lambda \frac{dT}{dr} \tag{2.1}$$

In this law the heat flux, $\phi''_{q,r}$, is related to the 'driving' force, $\frac{dT}{dr}$, the temperature gradient. The heat conductivity coefficient, λ , is a material property. The minus sign is introduced to guarantee that heat always flow from places with a higher temperature to places with a lower temperature.

The heat flow per unit height, ϕ'_q , is obtained from the heat flux by multiplying it with the circumference, $2\pi r$, of the cylindrical area through which the heat flux flows.

$$\phi'_q = 2\pi r \cdot \phi''_q \tag{2.2}$$

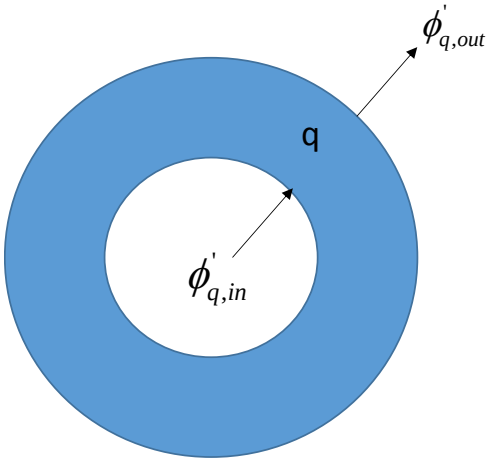

Figure 6 Coaxial ring to determine thermal energy balance

Under stationary conditions the temperature profile in the HTR-PM does not change. This means that, when looking at a coaxial ring in Figure 6, the thermal energy balance is given by:

$$\phi'_{q,in} + q - \phi'_{q,out} = 0 \tag{2.3}$$

In (2.3), *q* represents the produced heat by nuclear fission in the coaxial ring per unit height. Outside the reactor core the thermal energy balance over a coaxial ring reduces to:

$$\phi'_{q,in} = \phi'_{q,out} \tag{2.4}$$

In the helium gaps and the air gap, heat radiation is the dominant way of heat transfer. Heat radiation in a cylinder between two surface areas is described by Stefan-Boltzmann's law [7]:

$$\phi_{q,rad} = \varepsilon_n \sigma A_1 (T_1^4 - T_2^4) \tag{2.5}$$

In this equation, σ, is Stefan-Boltzmann's constant equal to $5{,}670373 \cdot 10^{-8} Wm^{-2}K^{-4}$. A_1 is the inner surface area. T_1 and T_2 are the temperatures of the inner and outer surface areas, respectively. ε_n is the system emissivity of the annular cavity between the inner and outer surface [7].

$$\varepsilon_n = \frac{1}{\frac{1}{\varepsilon_1} + \frac{A_1}{A_2}\left(\frac{1}{\varepsilon_2} - 1\right)} \tag{2.6}$$

A_2 is the outer surface area and, ε_1 and ε_2 are the emissivities of the inner and outer surface materials, respectively.

To determine the effective heat conductivity in the gas layers, λ_{eff}, the heat transfer contribution by conduction, λ_{cond}, and the heat transfer contribution by radiation, λ_{rad}, are added. The lambdas for radiation are deduced from (2.1) and (2.5).

$$\lambda_{eff} = \lambda_{cond} + \lambda_{rad} = \lambda_{cond} + \frac{\phi_{q,rad}}{\Delta T \cdot \Delta r} \tag{2.7}$$

In appendix B, the effective heat conductivities and the emissivities of the reactor components are listed. These coefficients describe the ability of a material to transfer heat by conduction and radiation, respectively.

2.4. The finite volume method

The finite volume method (FVM) [15,16] is a well-known method for spatial discretization in computational fluid dynamics (CFD). The FVM is used for evaluating partial differential equations in the form of simple algebraic equations. The two main advantages of the FVM in comparison to the finite difference method (FDM) are that the FVM provides a natural way of preserving conservative properties and the FVM is easier implemented in curvilinear coordinate systems [15].

The finite volume method uses a three step procedure to discretize partial differential equations.

Step 1) Divide the domain into a number of finite sized sub-domains, called control volumes.

Step 2) Integrate the governing differential equation over each control volume.

Step 3) Consider a profile assumption, linear or constant, for the dependent variable for evaluating the integrals of Step 2.

After this three step procedure the partial differential equation is discretized into a set of linear algebraic equations [12].

In case of a DLOFC event the governing differential equation is equal to the following heat equation in cylindrical coordinates:

$$\frac{\partial}{\partial t}\left(\rho c_p T\right) = \frac{1}{r}\frac{\partial}{\partial r}\left(r\lambda\frac{\partial T}{\partial r}\right) + S \tag{2.8}$$

In this equation $\frac{\partial}{\partial t}$ and $\frac{\partial}{\partial r}$ are the partial derivatives to time, *t*, and the spatial coordinate, *r*, respectively. ρ and c_p are the density and the specific heat capacity of the materials in the control volume, respectively, and *S* is the source term that represents the heat production in the control volume.

To validate the discretization of the FVM the temperature profiles of the steady state heat flux model and the steady state FVM are compared. In the steady state model the time-dependent term in (2.8) is equal to zero.

For the time-dependent discretization the fully implicit scheme is used. In the fully implicit scheme the solution for the dependent variable is obtained using the values of the current time step for the terms on the right-hand side of (2.8). In the fully explicit scheme only the values of the previous time step for the terms on the right-hand side of (2.8) are used to obtain the solution. The implicit scheme is used to ensure numerical stability.

The discretized equations obtained using the fully implicit scheme in the FVM form a tridiagonal system of equations. These can be solved using the tridiagonal matrix algorithm (TDMA) [16]. This algorithm is a simplified form of the Gaussian elimination method for solving tridiagonal systems of equations. In the TDMA the methods of forward elimination and backward substitution are used.

In appendix B, the densities and the specific heat capacities of the materials in the HTR-PM are listed.

2.5. Decay heat models

In a nuclear reactor, heat generation continues after reactor shutdown. When the control rods are inserted the nuclear chain reaction is stopped, but the fission products continue to decay and thus produce heat. If this decay heat is not removed properly accidents are likely to occur. In the HTR-PM the temperature limits of the reactor components might be exceeded, resulting in a possible release of nuclear material and core damage.

The amount of decay heat over time depends on the concentration and composition of the fission products and actinides in the nuclear reactor. Statistical predictions of the composition of these fission fragments are given in so called yield curves. The fissile isotopes U-233, U-235 and Pu-239 have different yield curves, as shown in Figure 7.

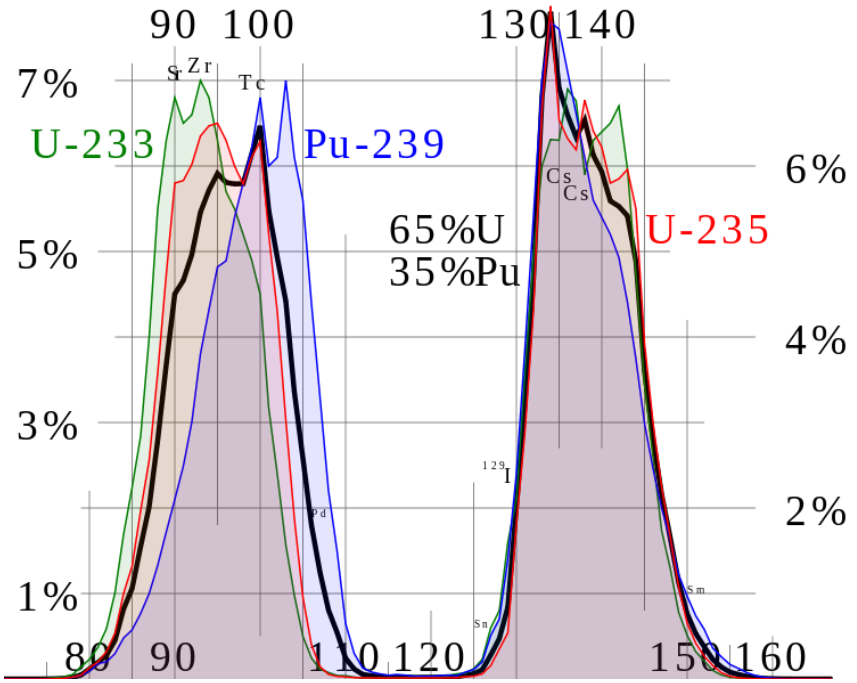

Figure 7 Yield curves of U-233 (green), U-235 (red), Pu-239 (blue) and a mixture of uranium and plutonium (black). Source: www.atomicinsights.com

Two models that approximate the decay heat of U-235 over time are the Way-Wigner approximation and the ANS-5.1 1993 model [18]. The ANS-5.1 model makes uses of 23 exponentials. The Way-Wigner approximation is given by the formula:

$$\eta(t) = 0.0622(t^{-0.2} - (t_0 + t)^{-0.2}) \tag{2.9}$$

In this formula η is the decay heat fraction, t is the elapsed time after stopping the fission chain reaction and t_0 is the time the fuel has been irradiated at nominal power in seconds [11]. In Figure 8, both decay heat models are shown for U-235. Initially the decay heat fraction of the ANS model is

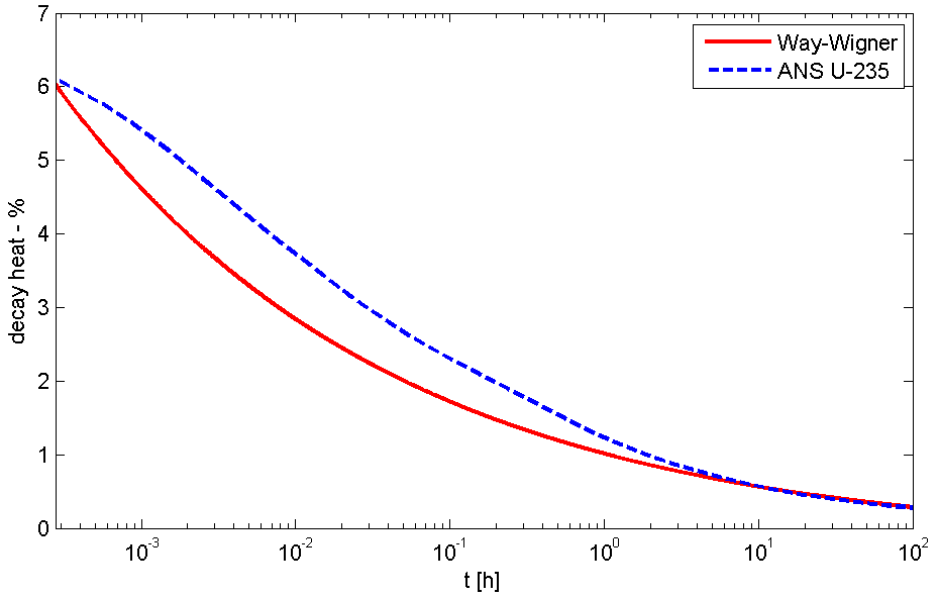

Figure 8 Decay heat fraction of U-235 the first 100 hours after a fuel irradiation time of 365 full power days, using both the Way-Wigner approximation and the ANS-5.1 model

higher, but after eleven hours the decay heat fraction of the Way-Wigner approximation is higher, for a fuel irradiation time of 365 full power days.

As can be deduced from Figure 8, the initial decay heat for U-235 is approximately 6 percent of the normal operating power. For Pu-239 this is 5 percent. There is not much data available about decay heat models of U-233. The yield curve of U-233 looks similar to the yield curves of U-235 and Pu-239. Therefore it is probable that U-233 has a similar decay heat model. It is also taken into account that the initial decay heat falls out higher than 6 percent. For instance, U-233 could have an initial decay heat fraction of 7 percent. This will also be simulated to see how it effects the maximum temperatures.

Chapter 3 Numerical methods

3.1. Steady state heat flux model

In this thesis, one-dimensional models are used to describe the heat transfer in the radial direction. The boundary condition of the model is the temperature of the water-cooling panel, which has a fixed temperature of 70°C. Using (3.1), the steady state temperature profile in the HTR-PM is obtained. The space between the core center and the water-cooling panel is divided in *n* steps. T_1 and T_n are the temperatures at the core center and the water panel, respectively. The temperature at each step is described using the following equation:

$$T_i = T_{i+1} + \frac{\phi''_{q,i+1} \cdot \Delta r}{\lambda} \tag{3.1}$$

where $\Delta r = r_{i+1} - r_i$ and *i* runs from *n*-1 to 1, in steps of -1. The heat conductivity coefficients, λ's, are determined using a iterative procedure. These coefficients are temperature dependent. Initially the λ's are obtained using an estimation for the temperature profile. Iterations are performed for the λ's until the temperature profile converges.

The heat flux outside the reactor core under stationary conditions is given by:

$$\phi''_{q,i} = \frac{P_{decay}}{2\pi \cdot r_i \cdot H} \tag{3.2}$$

P_{decay} is the decay heat production in the reactor core. In the one-dimensional steady state model the heat flow at all radii outside the core equals the produced decay heat, so the heat flux decreases as the radius increases. Inside the core the heat flow decreases as *r* decreases, because less fuel elements are enclosed as *r* decreases. The energy balance over a coaxial ring inside the reactor core, Figure 6, looks like:

$$\phi''_{q,out} A_{out} = \phi''_{q,in} A_{in} + q_{decay} V \tag{3.3}$$

In (3.4) this is rewritten, using simple math, to obtain an expression for the heat flux inside the reactor core.

$$\begin{aligned} &\phi''_{q,i} A_i = \phi''_{q,i+1} A_{i+1} + q_{decay} V_i \rightarrow \\ &\phi''_{q,i} = \phi''_{q,i+1} \frac{A_{i+1}}{A_i} + q_{decay} \frac{V_i}{A_i} \rightarrow \\ &\phi''_{q,i} = \phi''_{q,i+1} \frac{r_{i+1}}{r_i} + q_{decay} \frac{r_i^2 - r_{i+1}^2}{2r_i} \end{aligned} \tag{3.4}$$

q_{decay} is the decay heat produced per cubic meter inside the reactor core.

This steady state model will serve as validation for the spatial discretization of the steady state model obtained by the finite volume method. For simplicity, a spatially uniform decay power density of 1 percent of the normal operating power profile is chosen. The power rating during normal operation equals 250 MW_{th}.

3.2. Finite volume method

In Figure 9 the geometry of the control volume in cylindrical coordinates is defined. This elementary control volume is equal to:

$$dV = r\Delta r\Delta\theta\Delta z \tag{3.5}$$

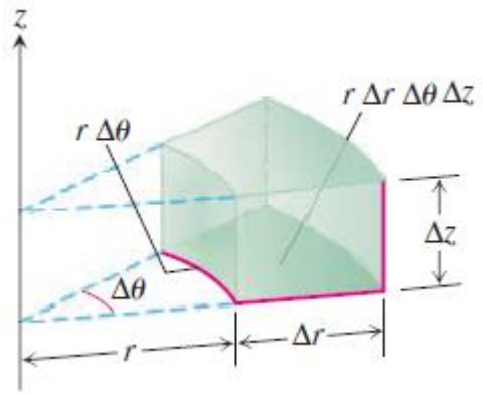

Figure 9 A control volume in cylindrical coordinates

The next step is to integrate the governing differential equation (2.8) over each control volume. Since no variations in $\Delta\theta$ and Δz are considered in this thesis these cancel out in all terms when integrated. A one-dimensional control volumes is shown in Figure 10.

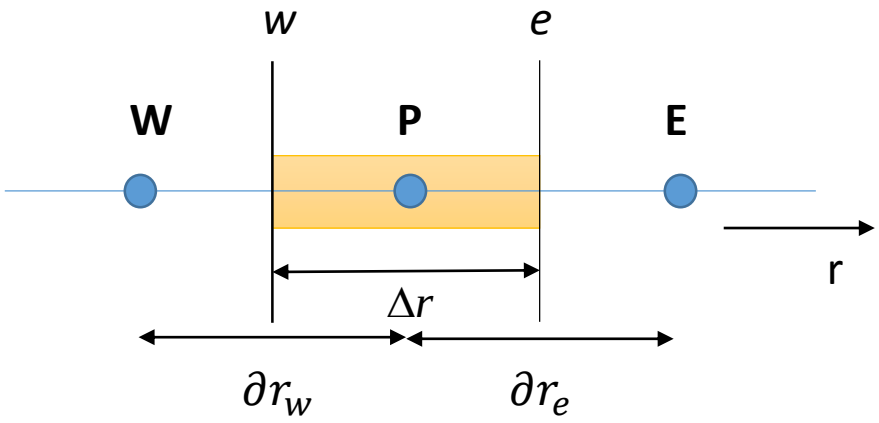

Figure 10 A one-dimensional control volume in the radial direction

In Figure 10, the shaded region represents a control volume. The grid-points are indicated by the capital letters W, P and E. The lower-case letters, w and e, indicate the west face and the east face of the control volume, respectively. Δr is the size of the control volume. δr_e and δr_w are the distances between the grid-points W and P and the grid-points P and E, respectively.

For this control volume, the following integral can be obtained when (2.8) is integrated over time and the spatial coordinate, *r*:

$$\int_{r_w}^{r_e}\int_{t}^{t+\Delta t}\frac{\partial}{\partial t}\left(\rho c_p T\right)rdtdr=\int_{t}^{t+\Delta t}\int_{r_w}^{r_e}\frac{1}{r}\frac{\partial}{\partial r}\left(r\lambda\frac{\partial T}{\partial r}\right)rdrdt+\int_{t}^{t+\Delta t}\int_{r_w}^{r_e}Srdrdt \tag{3.6}$$

The terms in (3.6) will be evaluated separately. For term 1 integration over time is straightforward. This results in:

$$\int_{r_w}^{r_e}\left\{\left(\rho c_p T\right)^{t+\Delta t}-\left(\left(\rho c_p T\right)^{t}\right)\right\}rdr \tag{3.7}$$

The next step is to integrate the temperature in the r-domain. If the temperature is integrated in the r-domain a piecewise constant profile assumption is made. On the other hand, if a derivative of the temperature with respect to *r* is integrated over time a piecewise linear profile assumption is made, since in case of a piecewise constant profile assumption the derivative would be zero.

Now integration in the r-domain results in:

$$\rho c_p(T_p^{\,t+\Delta t}-T_p^{\,t})\cdot(\frac{r_e^{\,2}-r_w^{\,2}}{2}) \tag{3.8}$$

For term 2 integration over *r* is straightforward, resulting in:

$$\begin{aligned}&\int_{t}^{t+\Delta t}\left\{\left(r\lambda\frac{\partial T}{\partial r}\right)_{r_e}-\left(r\lambda\frac{\partial T}{\partial r}\right)_{r_w}\right\}dt\rightarrow\\&\int_{t}^{t+\Delta t}\left\{\left(r_e\lambda_e\frac{T_E-T_P}{\delta r_e}\right)-\left(r_w\lambda_w\frac{T_P-T_W}{\delta r_w}\right)\right\}dt\end{aligned} \tag{3.9}$$

In (3.9) a piecewise linear profile is assumed for the temperature over *r*.

For integration of temperature over time the following profile assumption is made [15]:

$$\int_{t}^{t+\Delta t}Tdt=\left[\left(1-f\right)\cdot T^{t}+f\cdot T^{t+\Delta t}\right]\cdot\Delta t \tag{3.10}$$

In (3.10), *f* is a weighting factor. For specific values of *f* different time integration schemes can be derived [15].

Using (3.10) the evaluation of term 2 is completed:

$$\begin{aligned}&\Big[\ \frac{r_e}{\delta r_e}\left\{\left(\lambda_e\left(1-f\right)\cdot T_E\right)^{t}+\left(\lambda_e f\cdot T_E\right)^{t+\Delta t}\right\}-\frac{r_e}{\delta r_e}\left\{\left(\lambda_e\left(1-f\right)\cdot T_P\right)^{t}+\left(\lambda_e f\cdot T_P\right)^{t+\Delta t}\right\}\\&-\frac{r_w}{\delta r_w}\left\{\left(\lambda_w\left(1-f\right)\cdot T_P\right)^{t}+\left(\lambda_w f\cdot T_P\right)^{t+\Delta t}\right\}+\frac{r_w}{\delta r_w}\left\{\left(\lambda_w\left(1-f\right)\cdot T_W\right)^{t}+\left(\lambda_w f\cdot T_W\right)^{t+\Delta t}\right\}\ \Big]\cdot\Delta t\end{aligned} \tag{3.11}$$

Term 3 is first integrated in the r-domain and secondly over time. For the source term integration over *r*, a piecewise constant profile assumption is made and for the source term integration over time a similar assumption is made as (3.10).

$$\int_{t}^{t+\Delta t} S(t)\cdot\frac{r_e^{\,2}-r_w^{\,2}}{2}\,dt \rightarrow \frac{r_e^{\,2}-r_w^{\,2}}{2}\cdot\left[(1-f)\cdot S^{t}+f\cdot S^{t+\Delta t}\right]\cdot\Delta t \tag{3.12}$$

The evaluated terms can now be written in the form:

$$a_P T_P = a_E T_E + a_W T_W + a_P^0 T_P^0 + b \tag{3.13}$$

For notational convenience the temperatures at the current time step, $t+\Delta t$, are denoted by *T* and temperatures at the previous time step *t* are denoted by T^0. Now the subscripts indicating the grid points *W, P,* and *E* are replaced by *i – 1 , i* and *i + 1*, respectively. For the time discretization, a fully implicit scheme is chosen, because this results in unconditionally stable solutions. In a fully implicit scheme, *f* = 1, and this in combination with the evaluated terms and (3.13) gives:

$$a_i T_i = b_i T_{i+1} + c_i T_{i-1} + a_i^0 T_i^0 + d_i \tag{3.14}$$

In Equation (3.15) the coefficients are described.

$$b_i = \left(\frac{r_e\lambda_e}{\delta r_e}\right)_i,\quad c_i = \left(\frac{r_w\lambda_w}{\delta r_w}\right)_i,\quad a_i^0 = \left(\rho c_p\frac{r_e^{\,2}-r_w^{\,2}}{2\Delta t}\right)_i,\ a_i = b_i + c_i + a_i^0,\ d_i = \left(S\frac{r_e^{\,2}-r_w^{\,2}}{2}\right)_i \tag{3.15}$$

The next step is to solve the linear equation using the tridiagonal matrix algorithm [16]. Equation (3.14) is rewritten to:

$$T_i = P_i T_{i+1} + Q_i \tag{3.16}$$

$$\text{where}\quad P_i = \frac{b_i}{a_i - c_i P_{i-1}} \text{ and } Q_i = \frac{c_i Q_{i-1} + a_i^0 T_i^0 + d_i}{a_i - c_i P_{i-1}} \tag{3.17}$$

For each control volume *P* and *Q* are calculated using forward elimination. Subsequently, (3.16) is solved using backward substitution.

Chapter 4 Results

4.1. Steady state heat flux model versus the finite volume model

In the simulations of the depressurized loss of forced cooling events, instant depressurization to 1 bar and instant control rod insertion are assumed. Heat conduction and radiation are the dominant ways of heat transfer and heat transfer by convection is neglected. Figure 11 shows, the radial temperature profiles of the heat flux model and the finite volume model. In both steady state models the decay heat is considered uniform and time-independent at one percent of the normal operating power of 250 MW_{th}. In these steady state simulations, it can be seen that the temperature profiles exactly coincide. This is important for the confidence in the correctness of both models. From the figure it can be seen that the maximum fuel temperature exceeds the safety limit of 1600 °C for which the fuel elements can be retained in the TRISO particles. The reason for this high temperature beyond the safety limit is the unrealistic, relatively high decay heat power density of one percent that is assumed. During a DLOFC transient the decay heat production is already less than one percent after little more than an hour after control rod insertion. For now this does not matter, since the steady state models served as a first insight in the temperature profile and as a validation for the spatial discretization of the finite volume model.

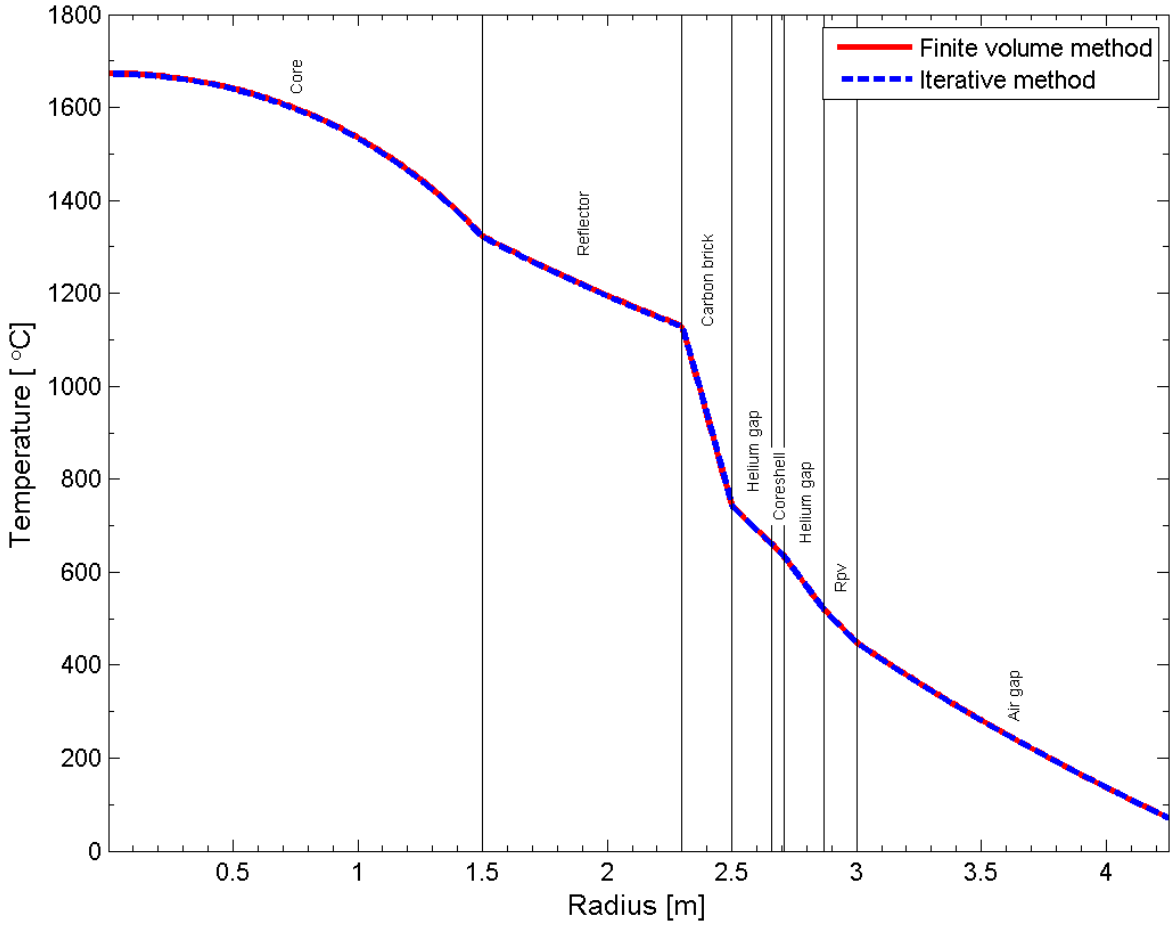

Figure 11 Steady state radial temperature profile for a decay heat production of 1% of the nominal power in the uranium fueled HTR-PM, obtained using the heat flux model and the finite volume model

4.2. Validation of the uranium fueled HTR-PM model

In Figure 12, the maximum fuel element temperature is illustrated over time after the DLOFC event. A similar study by Zheng et al. [7] using THERMIX is represented by the thick line in Figure 13. For the initial conditions, the steady state temperature and power density profile of Zheng's THERMIX model are used at around 2.75 m below the top of the core. At this height the power density distribution is maximum during steady state operation and this is where the maximum temperature is reached in Zheng's model and also in the MATLAB model. At this height most decay heat is produced, so this is where the maximum temperature is reached. Time steps of 5.8 seconds are used, because smaller time steps did not change the results and cost a lot more computational time.

From the figures, it can be seen that at time zero the steady state maximum fuel element temperature in the MATLAB model is approximately 500 °C, compared to 900 °C in the THERMIX model. The explanation for this is that the THERMIX model is two dimensional (*r*,*z*). At the beginning of the DLOFC transient, the maximum fuel element temperature is located near the core bottom. The coolant flows down through the core and at the bottom the coolant is already heated up, therefore the steady state temperature is higher. During the DLOFC event, the position of the fuel elements with the highest temperature moves towards the height where most decay heat is produced, around 2.75 m below the top of the core.

After the depressurization event the core starts to heat up as more decay heat is produced than removed by the residual heat removal system (RHRS). In the MATLAB model the maximum fuel temperature of 1269 °C is reached after 90 hours, compared to a peak value of 1492 °C after 26 hours [7]. From then on, as the decay heat production decreases, the maximum fuel temperature decreases slowly.

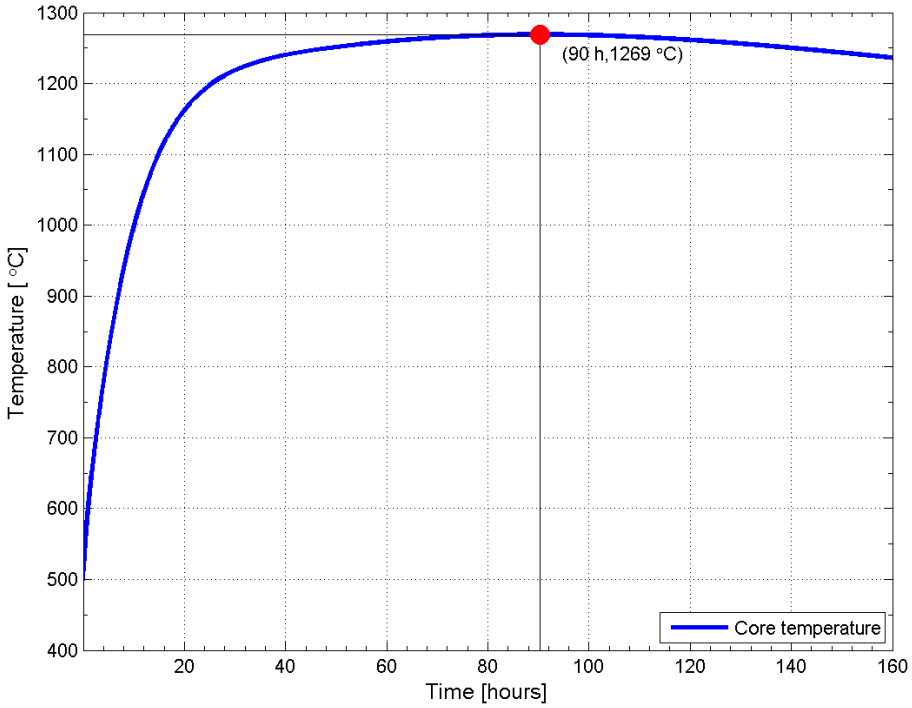

Figure 12 The maximum fuel element temperature over time during a DLOFC event in a uranium fueled HTR-PM, according to the FVM MATLAB model. The maximum temperature is 1269 °C reached after 90 hours. The maximum is indicated by the black lines and the red dot.

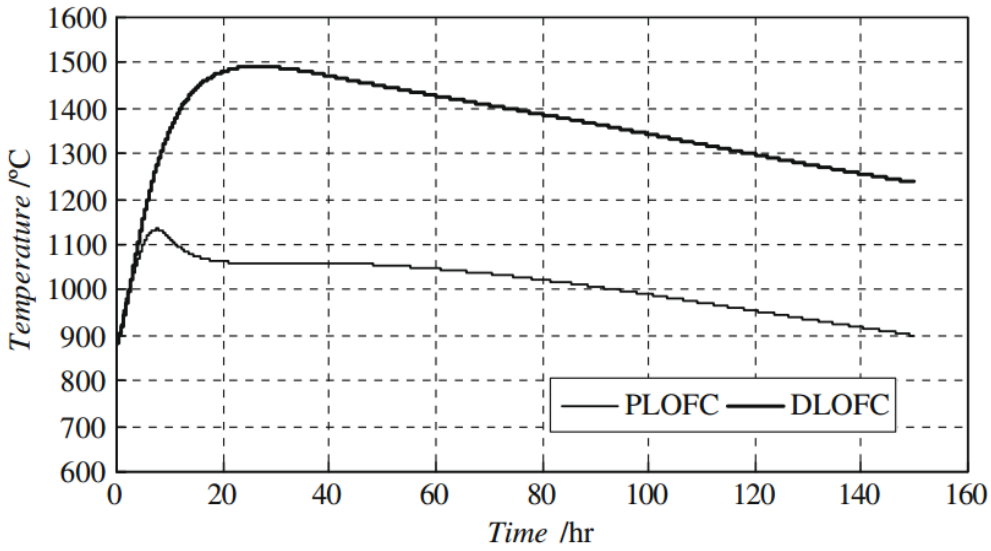

Figure 13 Reference for the maximum fuel element temperature over time during a DLOFC event in the uranium fueled HTR-PM, according to Zheng's model [7]. The maximum is 1492 °C reached after 26 hours.

In Zheng's model the maximum fuel element temperature is 223 °C higher and occurs 64 hours earlier. One would expect a higher maximum temperature in the MATLAB model, since here heat is transferred in the radial dimension only. Zheng uses a two-dimensional model (*r*,*z*), where the heat is also transferred in the axial direction. The difference in dimensionality is an important difference between the models.

The large difference between the models in maximum temperature and in the time after which the maximum is reached is difficult to explain. In the MATLAB model, the heat transfer from the fuel elements to the surface of the pebbles is neglected [7]. Also, the control rod channel, the leakage flow channel and the coolant channel in the reflector are neglected. The implementation of these channels and the temperature drop across the pebbles will reduce the temperature difference only slightly. One would have to take a closer look in Zheng's THERMIX model to see how the different layers and parameters are implemented. Differences in the core's emissivity coefficient or in other parameters in the Zehner-Schlunder formula influence the maximum temperature significantly, see Appendix B.

In Figure 14 and Figure 15 the heat loads of the RHRS of the MATLAB model and Zheng's model are shown. This heat load is approximated by the total heat flow near the water-cooling panel. This total heat flow is determined by multiplying the heat flux (2.1) by the area near the water-cooling panel. In the one-dimensional MATLAB model only the peak value of the power density is considered, since the model is one-dimensional. Therefore, the heat load in this model is multiplied by a factor to correct for this and to make the heat load comparable to the heat load in Zheng's model. This factor equals the average power density of the whole core divided by the radially averaged power density at 2.75 m below the top of the core, where the decay heat production is maximal.

The heat load in the MATLAB model is initially lower, approximately the first 50 hours, but then it increases substantially in comparison with Zheng's model. Most probably the value for the heat load changes when the MATLAB model would be extended into two dimensions, since the radiative part of the heat conductivities used to determine the heat load depend on temperature to the fourth power. This might be a reason why the heat load of the RHRS in the MATLAB model exceeds the designed capability of 1.2 MW for each reactor module [7].

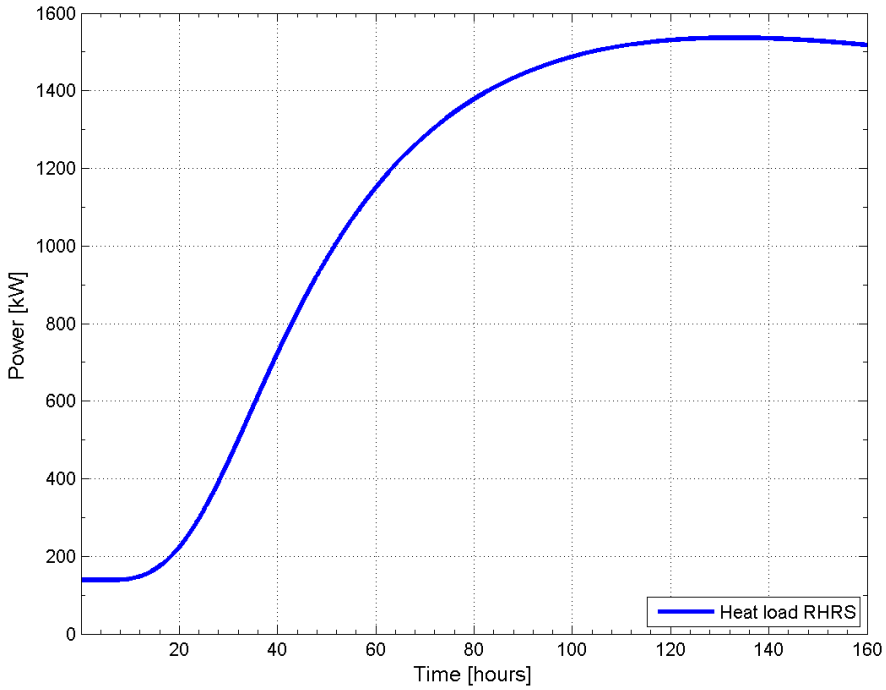

Figure 14 Heat load of the RHRS during the DLOFC event in the uranium fueled HTR-PM, according to the FVM MATLAB model.

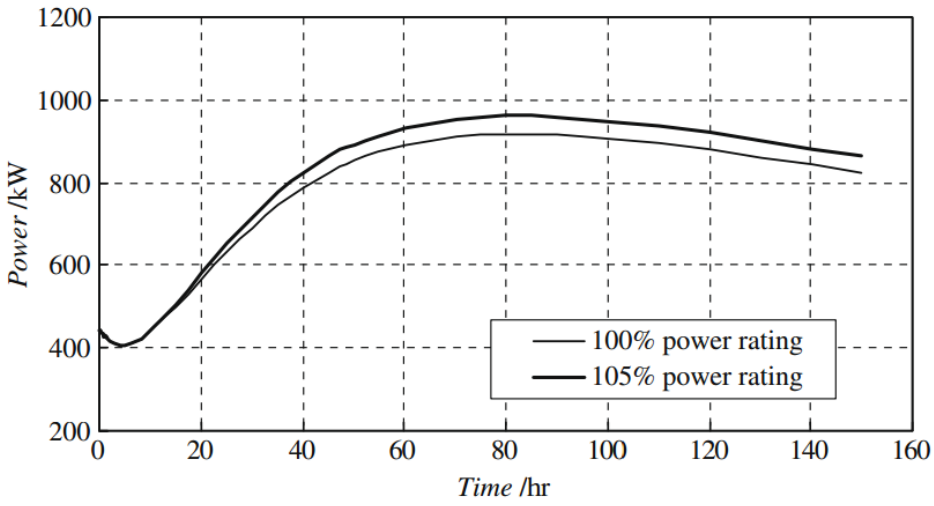

Figure 15 Reference for the heat load of the RHRS during the DLOFC event in the uranium fueled HTR-PM, according to Zheng's model [7].

Figure 16 indicates the radial temperature distribution in a uranium fueled HTR-PM fifty hours after the beginning of the DLOFC event. This temperature profile is compared with results from a similar transient study by Zheng et al. [7], represented by the blue line in Figure 17. This model will be referred to as the THERMIX model [7,20]. In the one-dimensional model, Zheng's power density profile in the middle of the core is used. The same initial temperature profile is used as in the steady state HTR-PM in Zheng's model. The decay heat production decreases according to the Way-Wigner approximation with an irradiation time of 1057 full power days (2.9). The temperature profiles look rather similar in shape, however, the core temperature profile and the inner helium gap's temperature profile differ most significantly. In Zheng's model the maximum fuel element temperature is 1400 °C compared to 1095 °C in the MATLAB model. Again, one would expect higher maximum temperatures in the one-dimensional model, where the heat is transferred in the radial direction only. The profile difference in the inner helium gap is difficult to explain since these differences are not observed in the outer helium gap.

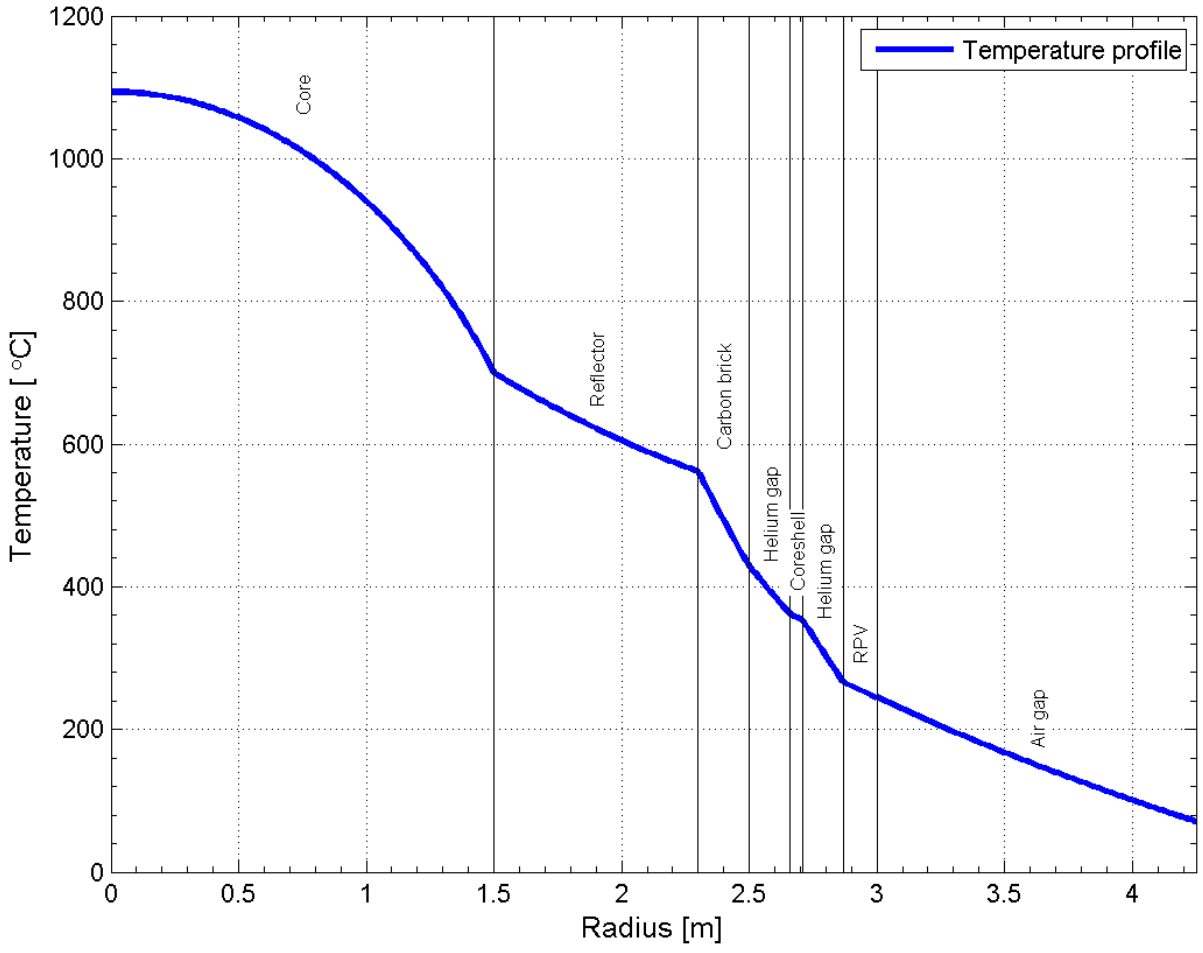

Figure 16 The radial temperature distribution in the middle of the core 50 hours after the beginning of the DLOFC event in a uranium fueled HTR-PM, according to the FVM MATLAB model.

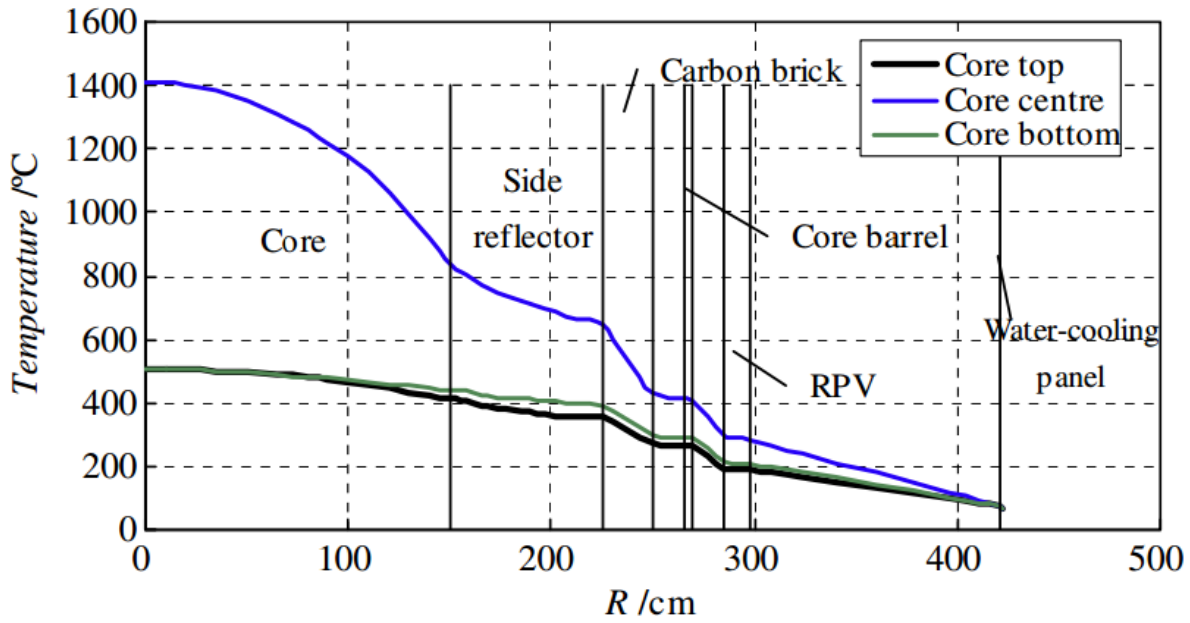

Figure 17 Reference for the radial temperature distribution in the middle of the core 50 hours after the beginning of the DLOFC event in a uranium fueled HTR-PM, according to Zheng's model.

When the temperature profiles are compared quantitatively, it can be noticed that the magnitude of the temperature difference in most layers is similar. In the core this is not true. In the THERMIX model there is a temperature difference of approximately 600 °C compared to a difference of 400 °C in the MATLAB model. In both models the Zehner-Schlunder and Robold synthetical formula [7] is used for the equivalent heat conductivity of a uniform pebble-bed. In the MATLAB model the heat transfer from the fuel elements to the surface of the pebbles is not considered, but that will only make a small difference. It might be interesting to find out how the Zehner-Schlunder and Robold synthetical formula is implemented in THERMIX, since this is a cumbersome formula with many temperature dependent terms. In a sensitivity analysis later on it will be demonstrated how small deviations in the core's effective heat conductivity affect the core temperature. It seems reasonable that an implementation difference partly contributes to the observed differences between the models.

To get an insight into the sensitivity of the maximum temperatures during a DLOFC event, a parameter sensitivity analysis is performed. Differences between the models are observed in the temperature difference across the core and in the maximum fuel element temperature. It is plausible that these quantities are strongly influenced by the heat conductivity of the core, the density in the core, the specific heat capacity in the core and of course the amount of decay heat produced. In the sensitivity analysis these design parameters will be analyzed. In Table 1 in the theory, the temperature limits of the reactor components are shown.

1) Heat conductivity in the reactor core

The heat conductivity in the reactor core is given by the Zehner-Schlunder and Robold synthetical formula [7,20]. This formula takes the dominant heat transfer mechanisms into account for the equivalent heat conductivity of the uniform pebble-bed, these are conduction and radiation. In Table 2, the results of the sensitivity analysis are shown. The maximum temperature of the fuel elements, the RPV and the core shell are shown. Also, the maximum heat load of the RHRS and the time at which the maximum fuel element temperature is reached are shown.

Table 2 Sensitivity analysis of the heat conductivity of the uniform pebble-bed in the uranium fueled HTR-PM

Multiplier factor to the heat conductivity	1.5	1.25	1	0.75	0.5
Maximum fuel element temperature [°C] / time at which maximum temperature is reached [hours]	1173.7/96	1213.1/94	1269.0/90	1354.9/83	1504.4/77
Maximum RPV temperature [°C]	386.1	385.8	385.3	384.6	382.9
Maximum core barrel temperature [°C]	501.9	501.6	501.1	500.1	498.1
Maximum RHRS heat load [kW]	1530.9	1528.5	1524.6	1517.8	1503.3

When the heat conductivity is lower, the heat transfer to the water panel is reduced, resulting in higher maximum fuel element temperatures and a lower heat load of the RHRS. The maximum fuel temperature is reached sooner with slower heat transfer and the maximum temperatures of the RPV and the core shell are slightly lower.

2) The density in the core multiplied by its specific heat capacity $\left(\rho \cdot c_p\right)$

The density and the specific heat capacity used are taken from the THERMIX program manual [20]. In Table 3 the results of the sensitivity analysis are shown. When $\rho.C_p$ is lower the maximum fuel element temperature is higher, although this factor has less influence than the heat conductivity. The maximum fuel element temperature is reached much sooner, so this factor has a greater influence on time in comparison with the heat conductivity. The heat load of the RHRS increases significantly with a lower factor and the maximum temperatures of the RPV and the core shell increase slightly. The multiplier factors are chosen to get an insight into the sensitivity of the maximum temperatures, in case of wrong implementation of the parameters.

Table 3 Sensitivity analysis of the density in the core multiplied by its specific heat capacity in the uranium fueled HTR-PM

Multiplier factor to $\left(\rho \cdot c_p\right)$ in the core	1.5	1.25	1	0.75	0.5
Maximum fuel element temperature [°C] / time at which maximum temperature is reached [hours]	1233.1/119	1250.2/105	1269.0/90	1289.7/76	1312.8/61
Maximum RPV temperature [°C]	375.3	380.1	385.3	391.0	397.0
Maximum core barrel temperature [°C]	488.9	494.8	501.1	507.8	515.0
Maximum RHRS heat load [kW]	1437.7	1479.2	1524.6	1574.2	1628.2

3) The decay heat

For the decay heat fraction the Way-Wigner approximation is used. When this fraction is increased by 10% and 20% the maximum fuel element temperature increases by 57 °C and 113 °C, respectively. The maximum temperatures of the RPV rises by 18 °C and 35 °C, respectively. The core shell's temperature rises by 22 °C and 42 °C, respectively. The maximum fuel element temperature increases significantly when the decay heat increases, so in the safety margins this has to be taken into account. No data is found about how U-233 decay heat models differ from those of U-235.

In conclusion, the maximum temperatures obtained by the MATLAB model are significantly lower than the results obtained by Zheng's model. This is in contradiction with the expected higher maximum temperatures in the one-dimensional model. In order to get an understanding of the difference, one should look closer into the THERMIX model. The temperature profiles outside the reactor core look very similar for both models, which gives confidence in the MATLAB model.

4.3. Thorium breeder pebble-bed reactor

Figure 18 shows the radial temperature distribution in the thorium breeder pebble-bed reactor fifty hours after the beginning of the DLOFC event. For the initial conditions, the steady state temperature and power density profile of Wols' THERMIX model are used [14]. When this temperature profile is compared with the temperature profile in the uranium fueled HTR-PM after fifty hours, Figure 19, it can be noticed that the greatest difference in profile occurs in the reactor core. This is not strange, since the core geometry and the power density profile are different. The radius of the core is 1.8 m instead of 1.5 m. Furthermore, in the thorium reactor, the power density is lower in the breeder zone. These differences contribute to a larger temperature drop across the reactor core. The rest of the temperature profile, from the reflector to the water-cooling panel, looks very similar. The maximum fuel element temperature is approximately 30 °C higher in the thorium breeder reactor.

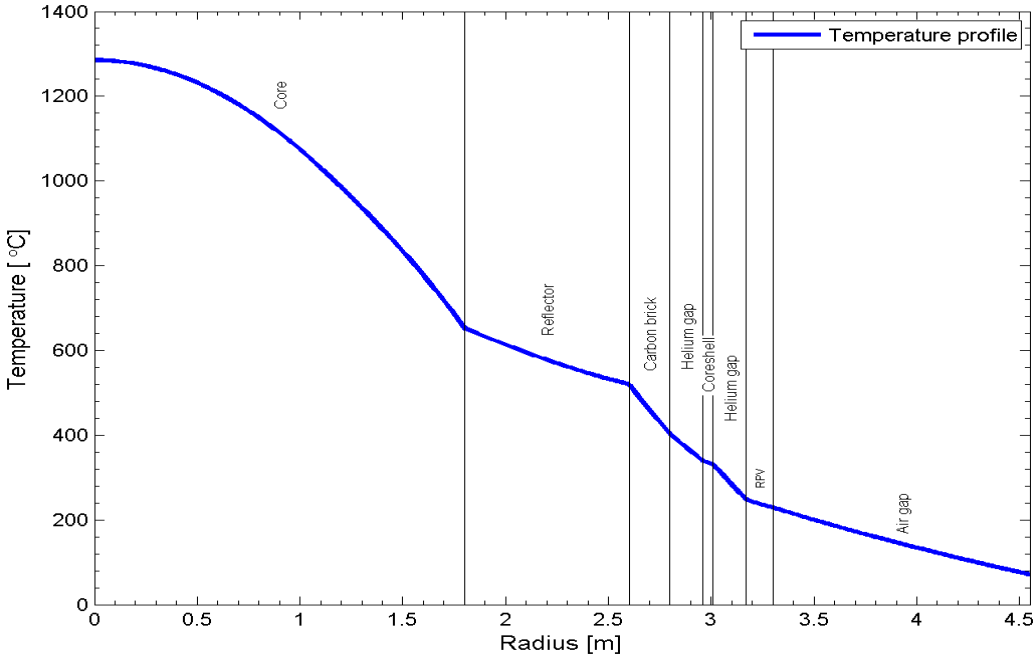

Figure 18 The radial temperature distribution 50 hours after the beginning of the DLOFC event in the thorium breeder pebble-bed reactor, according to the FVM MATLAB model. 1057 days is used for the fuel irradiation time and the height were the power density is maximal is modeled, around 50 cm above the middle of the core.

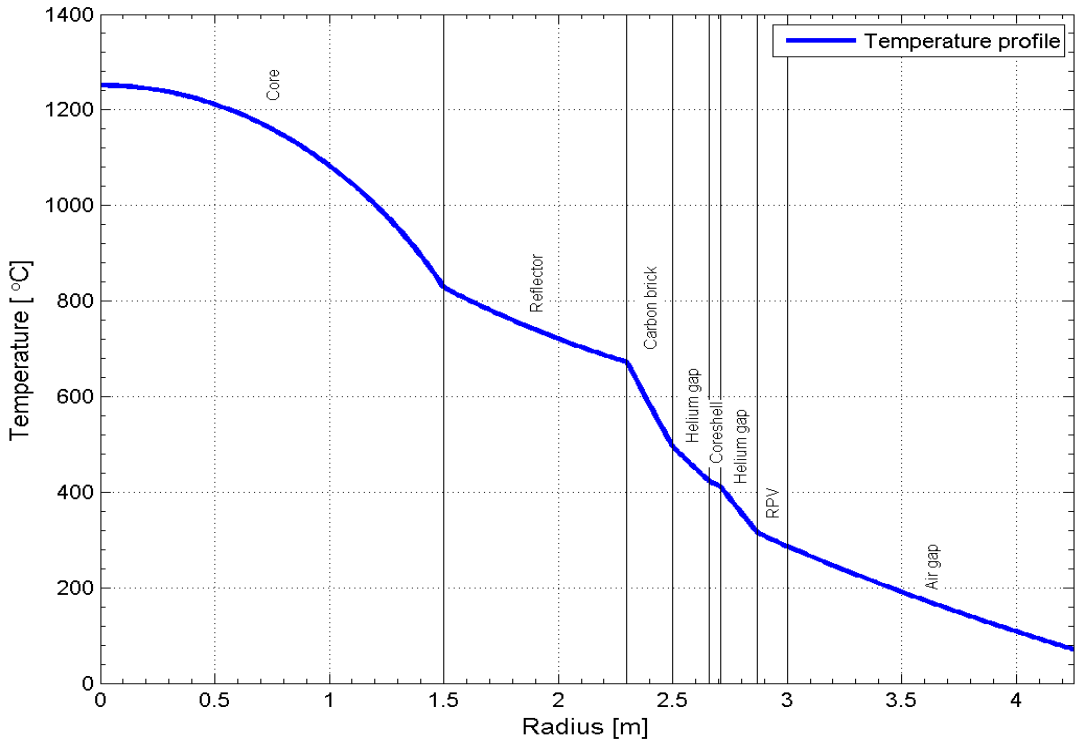

Figure 19 The radial temperature distribution 50 hours after the beginning of the DLOFC event in the uranium fueled HTR-PM, according to the FVM MATLAB model. 1057 days is used for the fuel irradiation time and the height were the power density is maximal is modeled, around 2.75 m below the top of the core.

In Figure 20 the maximum fuel element temperature is shown over time after the DLOFC event for the thorium breeder PBR. A similar study by Wols [14] in THERMIX is represented by the dashed line in Figure 21. The fuel irradiation time is set to 365 full power days in the Way-Wigner approximation, since this is the value Wols uses. In the thorium breeder pebble-bed reactor the maximum fuel element temperature is obtained 50 cm above the middle of the core, where the power density distribution is maximum during steady state operation. The steady state temperature at zero time is higher in the THERMIX model for the same reason as with the uranium fueled HTR-PM. The maximum fuel element temperature in the MATLAB model is 1244 °C and it is reached after 42 hours. In the THERMIX model the maximum temperature is 1572 °C which is reached after approximately 30 hours.

The maximum fuel element temperature profiles in the thorium breeder PBR's look very similar to the profiles in the uranium fueled HTR-PM's. After depressurization the core starts to heat up until a maximum temperature is reached. From then on, more heat is removed by the RHRS than produced by the fission fragments, so the temperatures start to drop.

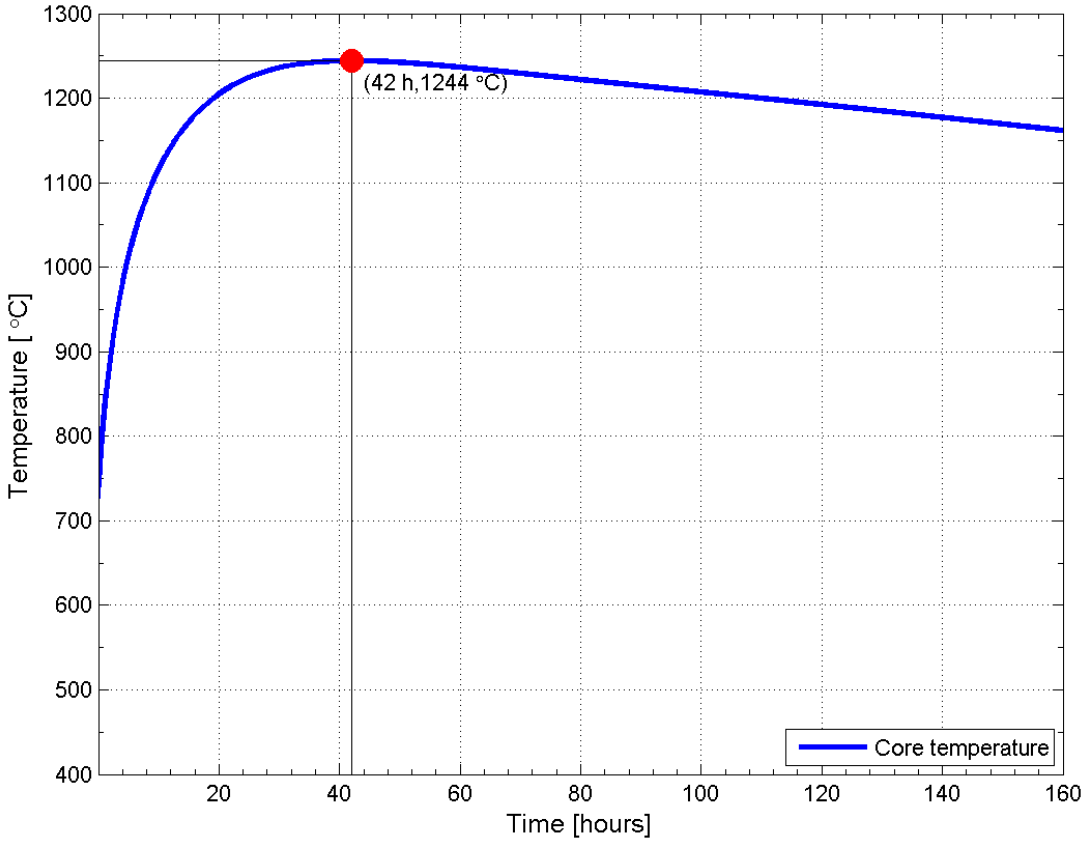

Figure 20 Maximum fuel element temperature during the DLOFC event in the thorium breeder pebble-bed reactor, according to the FVM MATLAB model. This time, 365 days is used for the fuel irradiation time, in accordance with the model by WOLS. The maximum temperature is 1244 °C reached after 42 hours.

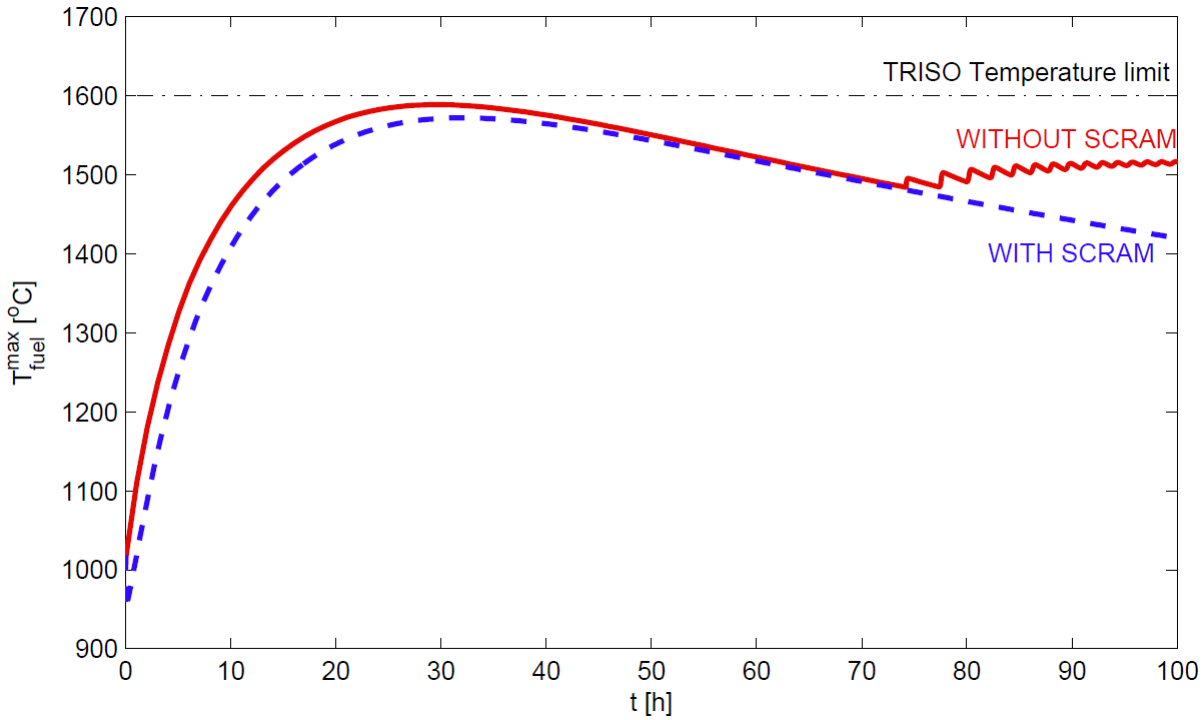

Figure 21 Maximum fuel element temperature during the DLOFC event in the thorium breeder pebble-bed reactor, according to Wols' model. 365 days is used for the fuel irradiation time. The maximum temperature is 1572 °C reached after approximately 30 hours.

In Table 4, it is shown how different decay heat models influence the maximum temperatures of the fuel elements, the RPV and the core barrel. In the Way-Wigner approximation three different initial decay heat fractions are chosen, 6%, 6.5% and 7%. When the initial fraction is increased from 6% to 7% the maximum fuel element temperature increases with 80 ^{o}C, which corresponds to a significant temperature increase of 6.4%. In the ANS-5.1 model the initial decay heat fraction is higher for the first eleven hours compared with the Way-Wigner (6%) model, for a fuel irradiation time of 356 days. The maximum fuel element temperature, however, is 6 ^{o}C lower and it is reached 8 hours earlier.

Table 4 Maximum temperatures in the critical reactor components of the thorium breeder pebble-bed reactor for different decay heat models

Decay heat model	Way-Wigner (6%)	Way-Wigner (6.5%)	Way-Wigner (7%)	ANS-5.1
Maximum fuel element temperature [^{o}C]	1244.2	1279.6	1323.8	1238.0
Time at which maximum temperature is reached [hours]	42	42	41	34
Maximum RPV temperature [^{o}C]	310.8	321.0	333.7	308.3
Maximum core barrel temperature [^{o}C]	409.5	422.0	437.6	406.4

For the fuel irradiation time 365 days is used. When 1057 days would be used the maximum fuel temperatures are approximately 30 ^{o}C higher. The maximum temperatures in the thorium breeder PBR are lower compared with the maximum temperatures of the uranium fueled HTR-PM, in the MATLAB models. On the other hand, when Zheng's model is compared to Wols' models, the maximum fuel element temperature is approximately 80 ^{o}C higher in Wols' model.

The maximum temperatures in Table 4 do not exceed the temperature limits of the reactor components, as stated in Table 1 in the theory. However, it is hard to draw a conclusion from this since the maximum temperature in Wols' model is 328 ^{o}C higher, see Figure 20 and Figure 21. With this difference in mind, the fuel elements would exceed the safety limit of 1600 ^{o}C for initial decay heat fractions of 6.5% and 7%. If it turns out that the maximum temperature in the thorium breeder pebble-bed reactor exceeds the safety limit, the reactor design parameters should be adjusted. For instance, a smaller reactor core or a lower operating power can be considered then.

Chapter 5 Conclusions and recommendations

Future reactor designs are only interesting for worldwide implementation when they are inherently safe. The reactor should be able to remove the decay heat by passive means only. In this thesis a uranium fueled HTR-PM and a thorium breeder pebble-bed reactor are studied. The main question is whether the thorium breeder pebble-bed reactor remains inherently safe in case of a depressurized loss of forced cooling (DLOFC) event. In a DLOFC event heat transfer by convection is negligible, so the decay heat must be removed by heat conduction and radiation. For this purpose, two one-dimensional heat transfer models were developed in MATLAB; a steady state heat flux model and a time-dependent finite volume model. The heat flux model served to validate the spatial discretization in the finite volume method. For the time discretization a fully implicit scheme is used. The finite volume model is used for transient calculations.

The solid temperatures obtained for the uranium fueled HTR-PM differed from results by Zheng's models mostly inside the reactor core. Differences were expected since the THERMIX models are two-dimensional compared to the one-dimensional MATLAB models. However, common sense would expect higher temperatures in the MATLAB models since in this model heat is transferred only in the radial direction where the power density is maximal, whereas the THERMIX results by Zheng show higher temperatures. In the MATLAB model the temperature drop across a pebble is neglected, but this would not explain the significant differences. A reason for the difference might be a different implementation of the heat transfer parameters within THERMIX and the MATLAB models. This is hard to say since the THERMIX models were not examined in the present work. To see how the design parameters influence the maximum temperatures, a parameter sensitivity analysis is performed. The results showed that a lower heat conductivity coefficient, a lower density and a lower specific heat capacity of the core result in higher maximum temperatures reached at earlier times. An overestimation of these parameters in the MATLAB model might be a cause of the different results of the models.

The model for the thorium breeder pebble-bed reactor differed from the model for the uranium fueled HTR-PM mostly in the reactor core. In the thorium PBR there is a larger temperature increase across the core. The main reasons for this are the different geometry and the lower power density profile in the breeder zone of the core. This resulted in a slightly higher maximum fuel element temperature, but in larger safety margins in the RPV and the core barrel. When the MATLAB thorium PBR model is compared to the THERMIX model of Wols, similar conclusions can be drawn as for the HTR-PM. The maximum temperatures are lower, which is probably caused by a different implementation of the parameters. In the MATLAB model simulations were done with different decay heat models. The Way-Wigner approximations is used with different initial decay heat fractions and the ANS-5.1 model is used. In order to say something about whether the maximum temperatures exceed the safety limit, the margin with Wols' model has to be taken into account.

For further research it can be recommended to extend the MATLAB model into two dimensions. Furthermore, it is recommended to take a closer look into the THERMIX models. What values do the heat conductivities and other design parameters have in THERMIX and how are these implemented in THERMIX. For further research, it is also interesting to extend the parameter sensitivity analysis to the temperature of the water-cooling panel and the emissivities in the gas layers. Furthermore, it might be interesting to implement U-233 decay heat models when more data becomes available. Finally, to get an insight in the consequences of a DLOFC event in a dynamical model, the heat transfer model can be coupled to the dynamical models of Rik van Bremen [21] and David Sanchez [22].

Appendix

A) Reactor Parameters

Reactor dimensions	Design value HTR-PM (Uranium fueled)	Design value Thorium breeder PBR
Core height [m]	11.00	11.00
Core radius [m]	1.5	1.80
Reflector radius [m]	2.30	2.60
Carbon brick radius [m]	2.50	2.80
Heliumgap 1 radius [m]	2.66	2.96
Coreshell radius [m]	2.71	3.01
Heliumgap 2 radius [m]	2.87	3.17
RPV radius [m]	3.00	3.30
Airgap radius [m] (= inner radius water panel)	4.25	4.55
Reactor power (th) [MW]	250	250
Pebble diameter (d_{pebble}) [m]	0.06	0.06
DOSIS (fast neutron radiation dose) [10^{21} EDN]	1	1

B) Physical properties equations

The following equations are used in the numerical models for the densities multiplied by the specific heat capacities $\left[\frac{J}{m^3 K}\right]$ the heat conductivity coefficients $\left[\frac{W}{mK}\right]$ and emissivity coefficients in the HTR-PM [13]. The temperatures are in °C. T_0 = 273.15 and $T_K = T + T_0$. A more detailed description can be found in the THERMIX manual [20].

Core

$$\rho \cdot c_p = 1.75 \cdot (0.645 + 3.14 \cdot 10^{-3} \cdot T - 2.809 \cdot 10^{-6} \cdot T^2 + 0.959 \cdot 10^{-9} \cdot T^3) \cdot 10^6$$

$$\lambda = (1 - \sqrt{1-\varepsilon}) \cdot (\lambda_{He} + \varepsilon \cdot \lambda_{str}) + \sqrt{1-\varepsilon} \cdot (a \cdot \lambda_{kugel} + (1-a) \cdot \lambda_c),$$

$$\varepsilon(T < 600\,^oC) = 0.8, \varepsilon(600 < T < 1000\,^oC) = \frac{T - 600}{2000} + 0.8, \varepsilon(T > 1000\,^oC) = 1.0,$$

$$\lambda_{He} = 2.682 \cdot 10^{-3} \cdot T_K^{\,0.71 \cdot (1 - 2 \cdot 10^{-4} \cdot P)} \cdot (1 + 1.123 \cdot 10^{-3} \cdot P),$$

$$\lambda_{rad} = 4 \cdot \sigma \cdot d_{pebble} \cdot \psi \cdot T_K^{\,4},$$

$$\psi = \frac{1}{(2/\varepsilon) - 1}$$

$$a = 0.016,$$

$$\lambda_{kugel} = 0.076098 + 1.0917 \cdot 10^{-4} \cdot T - 0.0348 \cdot 10^{-6} \cdot T^2 + 0.0008 \cdot 10^{-8} \cdot T^3,$$

$$\lambda_c = 2 \cdot \frac{\lambda_{He}}{AN - AM} \cdot \left(\frac{B \cdot AN - AM}{(AN - AM)^2} \cdot \ln\left(\frac{AN}{AM}\right) - \frac{B-1}{AN - AM} - \frac{B+1}{2 \cdot AM} \cdot (1 - AN + AM) \right),$$

$$B = 1.25 \cdot \left(\frac{1-\varepsilon}{\varepsilon}\right)^{10/9}, AM = B \cdot \frac{\lambda_{He}}{\lambda_{kugel}}, AN = 1 + \frac{\lambda_{rad}}{\lambda_{kugel}}$$

Reflector

$$\rho \cdot c_p = 1.75 \cdot (0.645 + 3.14 \cdot 10^{-3} \cdot T - 2.809 \cdot 10^{-6} \cdot T^2 + 0.959 \cdot 10^{-9} \cdot T^3) \cdot 10^6$$

$$\lambda = 1.15 \cdot (1.5648 - 0.3162 \log(T + 100)) \cdot F \cdot 10^2,$$
$$F = F_1 / (Y - F_2) + F_3,$$
$$F_1 = -0.0054705 + 0.00038214 \cdot T / 1000 + 0.13487 (T / 1000)^2,$$
$$F_2 = -0.013951 + 0.12064 \cdot T / 1000 - 0.32955 (T / 1000)^2,$$
$$F_3 = -0.07264 + 0.41459 \cdot T / 1000 + 0.23149 (T / 1000)^2,$$
$$Y = DOSIS / 10$$

Carbon brick

$$\rho \cdot c_p = 1.55 \cdot (0.645 + 3.14 \cdot 10^{-3} \cdot T - 2.809 \cdot 10^{-6} \cdot T^2 + 0.959 \cdot 10^{-9} \cdot T^3) \cdot 10^6$$

$$\lambda = \left(0.05 + 0.03 \cdot 10^{-3} \cdot T\right) \cdot 10^2$$

$$\varepsilon = 0.9$$

Helium

$$\rho \cdot c_p = \frac{48.14 \cdot \frac{P}{T_K}}{1 + 0.4446 \cdot \frac{P}{(T_K)^{1.2}}} \cdot 5195$$

$$\lambda = 2.682 \cdot 10^{-3} \cdot T_K^{\,0.71 \cdot (1 - 2 \cdot 10^{-4} \cdot P)} \cdot (1 + 1.123 \cdot 10^{-3} \cdot P) + \lambda_{He,cond}$$

$\lambda_{He,cond}$ is the contribution to the heat transfer by radiation, which is described in Chapter 2.

Core shell and RPV

$$\rho \cdot c_p = (7800 - 0.4368 \cdot T) \cdot (402.777 + 0.2335 \cdot T - 0.0001 \cdot T^2)$$

$$\lambda = (0.135 + 1.8566 \cdot 10^{-4} \cdot T) \cdot 10^2$$

$$\varepsilon = 0.9$$

Air

$$\rho \cdot c_p = 1.2923 \cdot P \cdot \frac{T_0}{T_K} \cdot \left(1 - 3.88 \cdot 10^{-4} \cdot P \cdot \left(1 - 0.575 \cdot \left(\frac{|650 - T_K|}{T_0} \right)^{3.4} \right) \right)$$
$$\cdot \left(1000 - 0.115 \cdot T_K + 4.59 \cdot 10^{-4} \cdot {T_K}^2 - 2.06 \cdot 10^{-7} \cdot {T_K}^3 + 5.33 \cdot 10^{-12} \cdot {T_K}^4 \right)$$
$$\cdot \left(1 + 1.98 \cdot 10^{-3} \cdot (P - 1) \cdot \left(\frac{T_0}{T_K} \right)^{2.4} \right)$$

$$\lambda = (4.8 \cdot 10^{-3} + 7.36 \cdot 10^{-5} \cdot T_K - 1.18 \cdot 10^{-8} \cdot {T_K}^2 - 5.53 \cdot 10^{-13} \cdot {T_K}^3 + 2.13 \cdot 10^{-16} \cdot {T_K}^4)$$
$$\cdot (1 + 2.381 \cdot 10^{-3} \cdot (p - 1) \cdot \frac{{T_0}^2}{T_K}) + \lambda_{air,cond}$$

In () $\lambda_{air,cond}$ is the contribution to the heat transfer by radiation, which is described in Chapter 2.

Water panel

$$\varepsilon = 0.9$$

Bibliography

[1] International Energy Agency, World energy outlook 2013 factsheet

[2] World Nuclear Association, Number of nuclear reactors operable and under construction

[3] World Nuclear Association, Electricity Supplied by Nuclear Energy

[4] Nuclear heat for hydrogen production: Coupling a very high/high temperature reactor to a hydrogen production plant, Rachael Elder, Ray Allen, Progress in Nuclear Energy, 51(3):500–525, 2009

[5] Design aspects of the Chinese modular high-temperature gas-cooled reactor HTR-PM, Zuoyi Zhang, Zongxin Wu, Yuliang Sun, Fu Li, Nuclear Engineering and Design, 236(56):485 – 490, 2006

[6] Fuel pebble design studies of a high temperature reactor using thorium, F.J. Wols, J.L. Kloosterman and D. Lathouwers, Paper HTR2012-5-002, 2012

[7] Thermohydraulic transient studies of the Chinese 200 MWe HTR-PM for loss of forced cooling accidents, Yanhua Zheng, Lei Shi, Yujie Dong, Annals of Nuclear Energy, 36(6):742-751, 2009

[8] Current status and technical description of Chinese 2 x 250 MW_{th} HTR-PM demonstration plant, Zuoyi Zhang, Zongxin Wu, Dazhong Wang, Yuanhui Xu, Yuliang Sun, Fu Li, Yujie Dong, Nuclear Engineering and Design, 239(7):1212-1219, 2009

[9] High Temperature Gas Reactors: Assessment of applicable codes and standards, B.K. Mcdowell, M.R. Mitchell, R. Pugh, J.R. Nickolaus, G.L. Swearingen, PNNL-20869, October 2011

[10] Technical design features and essential safety-related properties of the HTR-module, G.H. Lohnert, Nuclear Engineering and Design, 121(2):259-275, 1990

[11] Advantages of going modular in HTRs, H. Reutler and G.H. Lohnert, Nuclear Engineering and Design, 78(2):129-136, 1984

[12] The design features of the HTR-10, Zongxin Wu, Dengcai Lin, Daxin Zhong, Nuclear Engineering and Design, 218(13):25-32, 2002

[13] World Nuclear Association, Nuclear power in China

[14] F.J. Wols, Analysis of depressurized loss of forced cooling transients in thorium breeder pebble bed reactors using a coupled DALTON/THERMIX code scheme, Internal report, October 2013

[15] Analysis and modelling of physical transport phenomena, K. Hanjalic, S. Kenjeres, M.J. Tummers, H.J.J. Jonker, ISBN: 9789065621665, VSSD

[16] Computational Fluid Dynamics, video lectures, Dr. Suman Chakraborty, Professor Department of Mechanical Engineering, Indian Institute of Technology, Kharagpur, https://www.youtube.com/watch?v=kwqoyuZTglQ

[17] Fysische Transportverschijnselen, Harrie van den Akker, Rob Mudde, ISBN: 9789065621863, VSSD, 1996

[18] Decay heat predictions: Experiments, Methods, Data. Integral validation and decay heat standards, J.L. Kloosterman, IRI-131-2000-005, July 2000

[19] MATLAB R2010b, matrix laboratory, programming language developed by MathWorks

[20] THERMIX, Pebble-bed analysis software, originally developed by the KFA-Jülich and later developed by INET (THERMIX manual is included)

[21] Rik van Bremen, Water ingress scenario analyses of a thorium fueled high temperature reactor, BSc thesis, TU Delft, NERA-131-2013-006

[22] David A. Rodriguez Sanchez, Safety analysis of a thorium-fueled high temperature gas-cooled reactor, MSc thesis, TU Delft, PNR-131-2012-014